PHYSICAL AND MATHEMATICAL MODELLING OF LADLE METALLURGY OPERATIONS

N. El-Kaddah and J. Szekely
Massachusetts Institute of Technology
Cambridge, Massachusetts 02139 USA

ABSTRACT

Experimental measurements are reported, on the velocity fields and turbulence parameters on a water model of an argon stirred ladle. These velocity measurements are complemented by direct heat transfer measurements, obtained by studying the rate at which ice rods immersed into the system melt, at various locations. The theoretical work undertaken involved the use of the turbulence Navier-Stokes equations in conjunction with the k-ε model to predict the local velocity fields and the maps of the turbulence parameters. These theoretical predictions were in reasonably good agreement with the experimentally measured velocity fields; the agreement between the predicted and the measured turbulence parameters was less perfect, but still satisfactory. The implications of these findings to the modelling of ladle metallurgical operations are discussed.

1. INTRODUCTION

During the past decade there has been a growing interest in the development and application of ladle metallurgy as a means of the finishing treatment of molten steel. Indeed some form of a ladle metallurgy step, such as argon stirring in order to achieve homogenization has become an established component of the overall steelmaking sequence,[1,4].

Parallel to the industrial develoments a great deal of useful research has been done on various aspects of ladle metallurgy. It is generally appreciated that apart from process chemistry the fluid flow phenomena, such as the flow patterns and the extent of agitation play a key role in determining the overall effic   of these operations. In general ladle

metallurgical systems may be agitated either by the injection of gas

streams or by the use of an electromagnetic force field.   In view of the

topic of this conference our attention will be restricted to gas bubble

driven circulation systems only, but within this framework we shall seek

to review recent efforts aimed at the better understanding of the behavior

of these systems through the use of

       mathematical modelling

       physical modelling

       plant scale experimentation.

In considering gas bubble driven circulation systems in general, such

as an argon stirred ladle, from the standpoint of transport phenomena we

are faced with three groups of problems:

(i) The definition of the gross features of the circulation system,

that is the overall flow patterns and the mixing time.

(ii) The definition of heat mass and momentum transfer between the

melt and the bounding surfaces, i.e. problems concerned with refractory

erosion, slag - metal reactions and oxygen transfer from the refractory

to the bath and finally

(iii) The description of the detailed structure of the turbulent flow,

such as the map of the turbulent energy dissipation which would be needed

to model deoxidation kinetics, the coalescence of inclusion particles

and in general the interaction between suspended particles and the melt.

In reviewing previous work, major advances have been made regarding

the definition of the overall flow patterns and the mixing times, through

the use of physical modelling and the application of various turbulence

models. [5-13] Indeed it may be stated with some confidence that these problems

are well understood for certain geometries would be essentially a routine

task.

As an illustration Fig. 1 shows a plot of the mixing time against the rate of energy dissipation (i.e. the total power input into the system) and it is seen that most systems of metallurgical interest may be reasonably well represented on this plot.

It should be noted that there are sound fundamental reasons why such an improved understanding of these systems was readily developed. As far as the circulation of these systems is concerned in the bulk the inertial terms represent the key factors, thus the overall flow field may be readily modelled (either mathematically or physically) even if the viscous (including the eddy phenomena) components are not accurately represented. This is a key feature of body force driven flows.

The situation is rather less satisfactory regarding the other two problem areas, namely fluid to wall (or slag - metal) transport and the definition of the fine structure of the flow. Notwithstanding their obvious practical importance, these aspects of the problem received very much less attention; while attempts have been made to extend the theoretical treatment to the explicit representation of these phenomena this work has to be regarded as largely tentative at this stage, because of the absence of hard corroborating evidence.

The purpose of the work to be described in this paper is to report on recent research addressed to these problems. The actual results will be presented under the following three headings:

(1) Mathematical Model Development
(2) Physical Modelling and the Comparison of the Measurements with Predictions

    (3)   Plant Scale Measurements

2. MATHEMATICAL MODELLING

In essence the gas bubble driven circulation system represents an axi-symmetrical turbulent recirculating flow problem of the type which has been tackled by numerous investigators, [5-8, 10-12] One of the main problems encountered in previous studies was to obtain a proper representation of the boundary between the gas bubble rich jet cone region and the bulk of the liquid, both in·terms of position and in terms of stating the proper boundary conditions for the velocity and the velocity gradients.

The following assumptions have been made in the developing of the fluid flow equations:

(1)   The two phase region was confined to a plume, the dimensions of which were determined experimentally, e.g. from the visual observation of the "break through zone". [8,10]

(2)   The two phase region was assumed to be homogeneous

(3)   The velocity and the momentum flux were assumed to be continuous across the jet cone (plume) boundary

(4)   The two dimensional, turbulent Navier-Stokes equations were used in conjunction with the k-ε model to represent the fluid flow field, which was considered to be driven by the density difference in the two phase region.

Assumptions (1)-(3) are illustrated in Fig. (2).

Within the framework of these assumptions the governing equations take the following form:

equation of continuity:

$$\frac{1}{r}\frac{\partial}{\partial r}(\rho r U_r) + \frac{\partial}{\partial z}(\rho U_z) = 0 \tag{1}$$

Momentum balance in the z-direction

$$\frac{1}{4}\frac{\partial}{\partial r}(\rho r U_r U_z) + \frac{\partial}{\partial z}(\rho U_z^2) = -\frac{\partial p'}{\partial z} + \frac{1}{r}\frac{\partial}{\partial r}[r\mu_{eff}\frac{\partial U_z}{\partial r}] \tag{2}$$

$$+2\frac{\partial}{\partial z}[\mu_{eff}\frac{\partial U_z}{\partial z}] + \frac{1}{r}\frac{\partial}{\partial r}(\mu_{eff}\ r\ \frac{\partial U_r}{\partial z}) + \rho g\bar{\alpha}$$

Momentum balance in the r-direction

$$\frac{1}{r}\frac{\partial}{\partial r}(\rho r\ U_r^2) + \frac{\partial}{\partial z}(\rho U_r U_z) = -\frac{\partial p'}{\partial r} + \frac{2}{r}\frac{\partial}{\partial r}[r\ \mu_{eff}\frac{\partial U_r}{\partial r}] \tag{3}$$

$$+\frac{\partial}{\partial z}[\mu_{eff}\frac{\partial U_r}{\partial z}] + \frac{\partial}{\partial z}[\mu_{eff}\frac{\partial U_z}{\partial z}] - \frac{2U_r\mu_{eff}}{r^2}$$

where

$$\rho = \rho_\ell\ ,\quad r > r_c \tag{4}$$

$$\rho = \bar{\alpha}\,\rho_g + (1-\bar{\alpha})\rho_\ell,\ r < r_c \tag{5}$$

It follows that for the purpose of modelling the whole domain

has been treated as a homogenous medium, but with a spatially variable

density. Using drift flux model which allows the slip between the

bubbles and the fluid, the quantity $\bar{\alpha}$ may be expressed as [14].

$$\bar{\alpha} = \frac{1}{2\pi}\frac{Q_g - \pi r_c^2\ \bar{\alpha}(1-\bar{\alpha})U_\infty}{\int_o^r rU_z dr} \tag{6}$$

where U_α is the rising velocity of a characteristic single bubble, which is estimated as 40 cm/s.

The boundary conditions for the equation of motion take the following form:

at the axis

$$U_r = 0 \; ; \quad r - 0 \tag{7}$$

$$\frac{\partial U_z}{\partial r} = 0 \; ; \quad r = 0 \tag{8}$$

at the walls

$$U_r = U_z = 0 \tag{9}$$

at the free surface

$$U_z = 0 \; ; \quad z = H \tag{10}$$

$$\frac{\partial U_r}{\partial z} = 0 \; ; \quad z = H \tag{11}$$

at the orifice

$$U_z = U_0 \; ; \quad r = 0 \; , \quad z = 0$$

$$\tag{12}$$

or $\quad U_z = 0 \; ; \quad r = 0 \; , \quad z > 0$

Eqs. (1-12) constitute the complete statement of the fluid flow problem except for the definition of effective viscosity. In the present case we used the well established k-ϵ model for computing the turbulent viscosity.[15,16]

3. PHYSICAL MODELLING AND THE COMPARISON OF MEASUREMENTS WITH PREDICTIONS.

3.1 The apparatus

The apparatus was so constructed to allow the convenient measurement of the velocity fields and the turbulence characteristics in a cylindrical tank containing water, which is being agitated by an ascending gas bubble stream.

In essence the apparatus consisted of a cylindrical tank, containing water which was agitated by a gas stream, introduced through the bottom of the container, via a centrally located orifice. This cylindrical tank was surrounded by a square tank, also filled with water, in order to eliminate the parallaxis effects in the optical measurements.

Fig. 3 shows a schematic sketch of the apparatus, which also indicates the principal dimensions of the container. Fig. 3 also shows the supporting and positioning assembly used for the melting of ice rods. The actual melting rate was determined using photographic technique.

A schematic outline of the apparatus as a whole is shown in Fig. 4, where it is seen that the measurements of the velocities and of the turbulence characteristics was accomplished through the use of a laser anemometer. A TSI Laser anemometer was used, employing a Spectrophysics No. 124, He-Ne laser. The anemometer was operated in a dual beam mode,

9

with a analysis of the forward scattered light.

The velocity measurements involved the use of essentially standard procedures commonly employed in laser anemometry. The Reynolds stresses were obtained by taking measurements regarding a certain direction and then displacing these by 45° following the relation:

$$\overline{U_i U_j} = \frac{1}{2}\left(\overline{U_1'^2} - \overline{U_2'^2}\right) \tag{15}$$

where $\overline{U_1'^2}$ and $\overline{U_2'^2}$ are the fluctuating velocities at $+45^\circ$ and -45° from the coordinates i and j.

The procedure for obtaining Reynolds stresses by such means is again well documented. [17]

3.2 Experimental Measurements and Computed Results

In this section we shall present a selection of the experimental measurements and these will be compared with the computed values of the corresponding parameters. The material to be presented will include information on the velocities, on the turbulent kinetic energy and on the Reynolds stresses.

The mean Velocity Field

Figs. 5a,b show a comparison between the experimentally measured and the theoretically predicted velocity fields. It is seen that the agreement between measurements and predictions is reasonably good. It should be noted that the use of k-ε model in conjunction with appropriate wall functions will give a significantly better agreement between the measurements and the predictions, especially in the near wall regions than would the use of simpler computational procedures, employing a single value of the effective viscosity. [10]

Figs. 6a,b,c shows a comparison between predicted and the measured absolute values of the velocity vector at three axial positions. It is seen that the agreement is quite reasonable throughout the domain.

Fig. 7 shows the computed velocity distribution in the jet cone region, which has been normalized with respect to the maximum (centerline) velocity. It is seen that this normalized axial velocity is essentially independent of the axial position. The Gaussian type distribution found seems to be in good agreement with the experimental measurements of Tse-Chang et al. [9] It is noted that measurements were also made of $\bar{U}_\theta$ which we found to be close to zero in all cases. However, as will be shown subsequently $\overline{U_\theta'^2} \neq 0$.

TURBULENCE CHARACTERISTICS OF THE SYSTEM

Fig. 8 shows the profiles of the rms velocity components normalized with respect to the mean velocity in the jet cone at the corresponding vertical position. A somewhat simplified analytical method was used for estimating the latter quantity. [11] The turbulence appears to be fairly isotropic except in the vicinity of the solid surfaces (side walls and the bottom), which is essentially in line with expectations. The other interesting feature of these results is the similarity exhibited by the plots shown in Figs. 9a, b.

Figs. 10a,c show a comparison between the experimentally measured and the calculated values of the turbulent kinetic energy. The agreement seems to be within about a factor of two in most cases, which is not unreasonable; but this discrepancy indicates that further study of these phenomena would be fully justified. This further theoretical work could involve either the adjustment of the parameters in the k-ε model or perhaps

12

3.3 HEAT TRANSFER AND PHASE CHANGE

In these series of experiments we studied the rate at which ice rods melt, upon immersion into a gas bubble agitated water pool. The main motivation for this work was to obtain a better insight into the effect of the velocity fields and the local turbulence parameters in the system on heat transfer between the fluid and an immersed solid body. These types of problems are of course of considerable practical interest both regarding wall erosion and dissolution kinetic.

Fig. 12 show typical photographs of the melting ice rods for various values of time.

Fig. 13, show typical plots of the position of the melting interface against time, obtained within the jet cone and outside the jet cone respectively. The near linearity of these plots indicates that the time required for the attainment of steady state melting conditions was relatively short. Figs. 14-18 show plots of the initial melting rate as a function of position within the agitated liquid.

Figs. 14 and 15 show the radial variation in the melting rate of two constant axial positions. It is seen that the melting rate is the highest in the jet cone and that it decreases quite rapidly with the radial distance from the axis of the gas jet.

Fig. 16 summarizes the radial variation in the melting rates at various axial positions in jet cone. The maximum melting rate is seen to occur at the center at an intermediate height; it may be shown that the fluid velocity is the maximum at this position.

Figs. 17 and 18 shows the axial variation of the melting rate for two fixed radial positions within the tank, one near the wall and the other in an intermediate position. Figs. 17 and 18 show a monotonous increase in the rate of melting with the distance from the bottom of the vessel. A sharp increase is observed on approaching the free surface. This behavior is attributable to the high level of turbulence in the vicinity of the free surface. Fig. 17 depicting the behavior of the system at an intermediate radial position, shows a minimum in the melting rate, corresponding to the center of the vortex, which of course, is a quiescent portion of the vessel.

4. PLANT SCALE MEASUREMENTS

At present there are only a limited number of plant scale measurements where sufficient details are available on the system to allow a meaningful comparison between the measurements and the predictions. Nonetheless it is important to cite these because they provide the ultimate test of the results obtained in the mathematical and water modelling work which has been described in the bulk of the paper.

4.1 Mixing

Mixing is the topic which has been the most extensively studied. Indeed numerous data are available on tracer dispersion and mixing a vessel of various size. [8,10,13] Since this field is now quite well understood, we shall present only one, typical example, illustrating that the theoretical predictions provide quite satisfactory answers regarding the mixing time. It should be noted that in most industrial scale systems, where the flow is reasonable turbulent, the dispersion of the tracer takes place by two

14

mechanisms, namely bulk convection and eddy diffusion. The actual

convective time scale is very short, in these systems, typically of the

order of a few seconds (linear dimensions being of the order of 1-2 m,

while the characteristic velocity being about 0.3 m/s). Thus the rate

determinine step in tracer dispersion or mixing will be eddy diffusion

between the respective streamlines with eddies of smaller time scale

(Kolmogoroff eddies $t \simeq (\nu/\epsilon)^{1/2} \simeq \cdot 1s$) as sketched in Fig. 19. This behavior

is of course consistent with the discussion presented in the introductory

section, concerning the fact that the mixing characteristics of a system

may be readily related to the total energy input.

4.2 Desulfurization Kinetics

Fig. 20 shows a sketch of a typical arrangement used for the desul-

furization of steel melts. [18] It is seen that a soli؛ desulfurization

agent is injected into the melt together with a carrier gas, through a

suitably placed lance. The overall rate of the desulfurization reactions

depends on two factors; in addition to the obvious criteria determined by

thermodynamic equilibria.

(i) The rate at which the individual particles react is determined

by the Kilmogoroff eddies, [19,21] which clearly depends on the local rate

of turbulent energy dissipation.

(ii) The rate at which the reactant, that is the sulfur is being

transported to the regions where the reaction is actually taking place.

As mentioned earlier, in connection with mixing, the rate of this transport

will be limited by eddy diffusion.

Figs. 21a, b, shows a comparison between the experimentally measured
and the theoretically predicted desulfurization rates, for a pilot scale
and an industrial scale system respectively. [18] It should be remarked,
that while these two sets of curves appear to be quite similar the actual
reaction mechanism differed substantially in the pilot scale and in the
full scale system.

In the pilot scale operation, where the system was heavily deoxidized,
the reaction took place in the plume, while in the industrial scale unit
which was not strongly deoxidized, most of the desulfurization took place
at the slag metal interface. The very good mixing which was provided by
the gas bubbles in the large scale system provided an adequate rate of
transport to the reactions zone.

4.3 Heat or mass Transfer to Immersed Surfaces

A key problem in the operation of ladle metallurgical operations
is the definition of the factors that govern wall erosion, and hence the
lining. Relatively little modelling work has been done in this area,
but a useful start has been made regarding the study of the rate at which
immersed bodies dissolve.

Fig. 22 shows a typical experimental arrangement, used at MEFOS in
the study of the rate at which immersed graphite rods would dissolve in
6 ton iron melts, and the actual experimental results are given in Fig. 23
in the form of the local mass transfer coefficients.

The numerical values of these mass transfer coefficients would be
difficult to predict from first principles (and the same applies to the wall
erosion rates) because the local fluxes at the solid surface will depend

not only on the local velocities but also on the turbulence levels in
the system. However, a preliminary prediction may be made regarding the
numerical values of these transfer coefficients through the appropriate
scaling of water modelling experiments, which were reported in Section 3.

Upon considering that the conditions of turbulence were comparable
in the water model system and the pilot scale experiments (indeed the
water models were designed with this objective in mind) the mass transfer
coefficients may be scales with the aid of the following formula:

$$N_{Nu} = 0.388 \ (N_{Re} Tu) N_{Pr} \qquad 100 < Re < 2000 \qquad Tu \gtrsim 13 \qquad \text{(13)}$$

The actual numerical values that one may obtain for the mass transfer
coefficient ranged from about 0.002-0.05 cm/s which compare reasonably
well with those found in the pilot scale, hot metal studies.

6. DISCUSSION

In the paper a brief review was presented of recent work concerned
with the mathematical and physical modelling of transport phenomena in
gas bubble driven circulation systems of interest in ladle metallurgy. This
modelling work was augmented by some plant scale measurements.

The present status of this effort may be summarized as follows:

(1) Through the statement of the two dimensional turbulent Navier-
Stokes equations and the proper boundaries conditions, the use of the
k-ε model provides an excellent representation of the overall flow field
and gives fairly good guidance regarding the spatial distribution of the
turbulence parameters.

(2) It must be realized that the k-ε model itself cannot predict the

local heat or mass transfer rates, but that these quantities have to be introduced in the form of the boundary conditions. In the absence of other reliable information these boundary conditions have to be deduced from semi-empirical correlations, which however do contain the computed velocity terms, some distance from the interface. It follows that the calculation of the local heat or mass transfer rates is neither empirical nor entirely fundamentally based, but is some compromise between these two extremes.

(3) Experimental measurements using water models and Laser Velocimetry have been very helpful in providing a rigorous test of these models. Indeed the above cited comparisons were based on these measurements. On combining the known velocity fields with the direct measurement of the local heat transfer rates, through the study of the rate at which ice rods melt in an agitated water pool valuable insight has been obtained. This work has clearly shown that in addition to the local velocities, the local turbulence levels also play a very important role in determining the local heat (or mass) transfer rates.

(4) At present only a limited number of plant scale measurements may be cited, which may be used for testing the predictions based on the model. However, the data available indicate that the combined approach using both physical and mathematical models appears to be very powerful.

(5) Clearly a number of problems remain unsolved and a great deal of further work would be desirable in a number of areas, in particular:

(i) It would be desirable to obtain a better understanding of the factors that govern the local heat and mass transfer rates between the bath and the wall and the bath and a slag cover.

(ii) It would be helpful to apply the known spatial distribution of the turbulent kinetic energy to develop more comprehensive models for deoxidation kinetics.

(iii) And finally, while the k-ϵ model has proven to be quite satisfactory, the development of an improved model, which has a sound theoretical basis should be a future long term goal.

ACKNOWLEDGEMENTS

List of Symbols

A	cross section of area of two phase region	m^2
g	acceleration due to gravity	m/s^2
H	right of the liquid column	m
k	turbulent kinetic energy	$(m/s)^2$
P	pressure	$kg/m.s^2$
P'	modified pressure, P-ρgz	kg/ms^2
Q	volumetric flow rate	m^3ls
r	radial coordinate	m
r_c	radius of two phase region	m
R	radius of the bath	m
U	velocity	m/s
U'	RMS velocity	
U_∞	rising velocity of a single bubble	m/s
z	axial coordinate	m
α	average void fraction of the gas in the two phase region	
ϵ	turbulent energy dissipation	m^2/s^3
μ	viscosity	kg/m.s
ν	kinematic viscosity	m^2/s
ρ	density	kg/m^3
λ	jet cone angle	

Subscripts

eff effective
g gas
ℓ liquid
O orifice
r radial direction
t turbulent
z axial direction 0 tangential direction

References

(1) Scaniject I. Proc. Int. Conf. Injection Metallurgy, MEFOS, Lulea Sweden, June, 1977.

(2) Scaniject II, Proc. Int. Conf. Injection Metallurgy, MEFOS, Lulea Sweden, June, 1980.

(3) McMaster Symposium on Ladle Treatment of Carbon Steel, Hamilton, Canada, Ed. J.S. Kirkaldy, May, 1979.

(4) W.G. Wilson and A. McLean, Desulfurization of Iron and Steel and Sulfide Shape Contro., Iron and Steel Society AIME, (1980).

(5) J. Szekely, H.Y. Wang and K.M. Kiser, Met. Trans. Vol 7B, 287, 1976.

(6) T. DebRoy, A.K. Majundar, D.B., Spalding, Appl. Math. Modelling 2, 146-150, 1978.

(7) J.W. McKelliget, M. Cross, R.D. Gibson and J.K. Brimacombe, ICHMT Int. Sem. on Heat and Mass Transfer in Met. Systems, Dubrovnik, Yugoslavia, Sept. 1979.

(8) J. Szekely, T. Lehner and C.W. Chang, Ironmaking and Steelmaking 1979, vol. 6, 285.

(9) H. Tse-Chang, T. Lehner and B. Kiellberg, Scand. J. Met., 1980, 9, 105.

(10) J. Szekely, N.H. El-kaddah and J.H. Grevet, Scaninject II, MEFOS 5:1, 1980.

(11) J.H. Grevet, J. Szekely and N.H. El-Kaddah, Int. J. of Heat and Mass Transf. In press.

(12) T. Deb-Roy and A.K. Majumdar, J. Metals 1981, Nov., 42.

(13) K. Nakanishi, T. Fujii and J. Szekely, Ironmaking and Steelmaking, 1975, 2, 193.

(14) G.B. Wallis, One Dimensional Two-Phase Flow, McGraw Hill, 1969.

(15) B.E. Launder and D.B. Spalding, Mathematical Models of Turbulence, Academic Press, 1972.

(16) B.E. Launder and D.B. Spalding, Computer Method Appl. Mech. Engg. 1974 3, 269.

(17) TSI, LDA Instruction Manual

(18) N.H. El-Kaddah, J. Szekely, Ironmaking and Steelmaking, 1981, 6, 269.

(19) R. Shinnar and J.M. Church, Ind. Engg. Chem. 1960, 52, 253.

(20) S. Middleman, AIChEJ., 11, 750, (1965).

(21) Y. Saro, N. Yamaguchi and T. Adachi, J. Chem. Engg. Japan, 1974,
      7, 255.

Table (1) Measured and Calculated Reynolds stresses $\overline{\rho U'_r U'_z}$
for 1.62 m/s. 1- measured 2-computed

z/H		r/R						
		0.90	0.80	0.70	0.60	0.44	0.28	0.14
0.98	(1)	-0.9	-7.2	-6.2	-3.2	-3.4	-	-
	(2)	-11.1	-16.3	-9.7	-5.2	+1.7		
0.93	(1)	+1. 6	+0.8	-2.6	-2.7	+2.5	-	-
	(2)	-3.4	-6.9	-5.6	-4.8	-2.7		
0.77	(1)	+5.0	+1.3	+0.5	+0.5	+2.3	-	-
	(2)	+3.0	+3.3	+1.7	+0.3	-0.2		
0.68	(1)	+3.7	+2.2	+0.6	+0.2	+0.9	+10.8	-
	(2)	+3.0	+4.7	+3.7	+2.3	+0.8	+1.4	
0.19	(1)	+0.3		+0.8	+1.1	+0.6	+0.4	+0.6
	(2)	+0.5	-	+0.7	+0.5	+0.2	+0.1	+0.9

Table 2 Measured and Calculated Reynolds stresses $\overline{\rho U'_r U'_z}$ for 3.2 m/s 1-measured 2-computed.

Z/H		r/R						
		0.90	0.80	0.70	0.60	0.44	0.28	0.14
0.98	(1)	+6.3	-7.5	-11.4	-8.4	-3.6	-	-
	(2)	-12.7	-25.1	-15.2	-8.6	+0.9		
0.93	(1)	+2.5	+2.5	-7.8	-4.1	+8.7	-	-
	(2)	-5.7	-10.7	-8.9	-7.7	-4.4		
0.77	(1)	+9.9	+3.0	+1.1	+1.1	+0.1	-	-
	(2)	+4.7	+5.4	+2.9	+0.5	-0.3		
0.68	(1)	+1.5	+4.1	+1.0	+0.3	+2.8	+44.4	-
	(2)	+4.9	+7.7	+6.1	+3.8	+1.3	+1.4	
0.19	(1)	+1.0		+3.8	+1.4	+2.2	+1.7	-0.9
	(2)	+0.8		+1.1	+0.8	+0.3	+0.2	+0.6
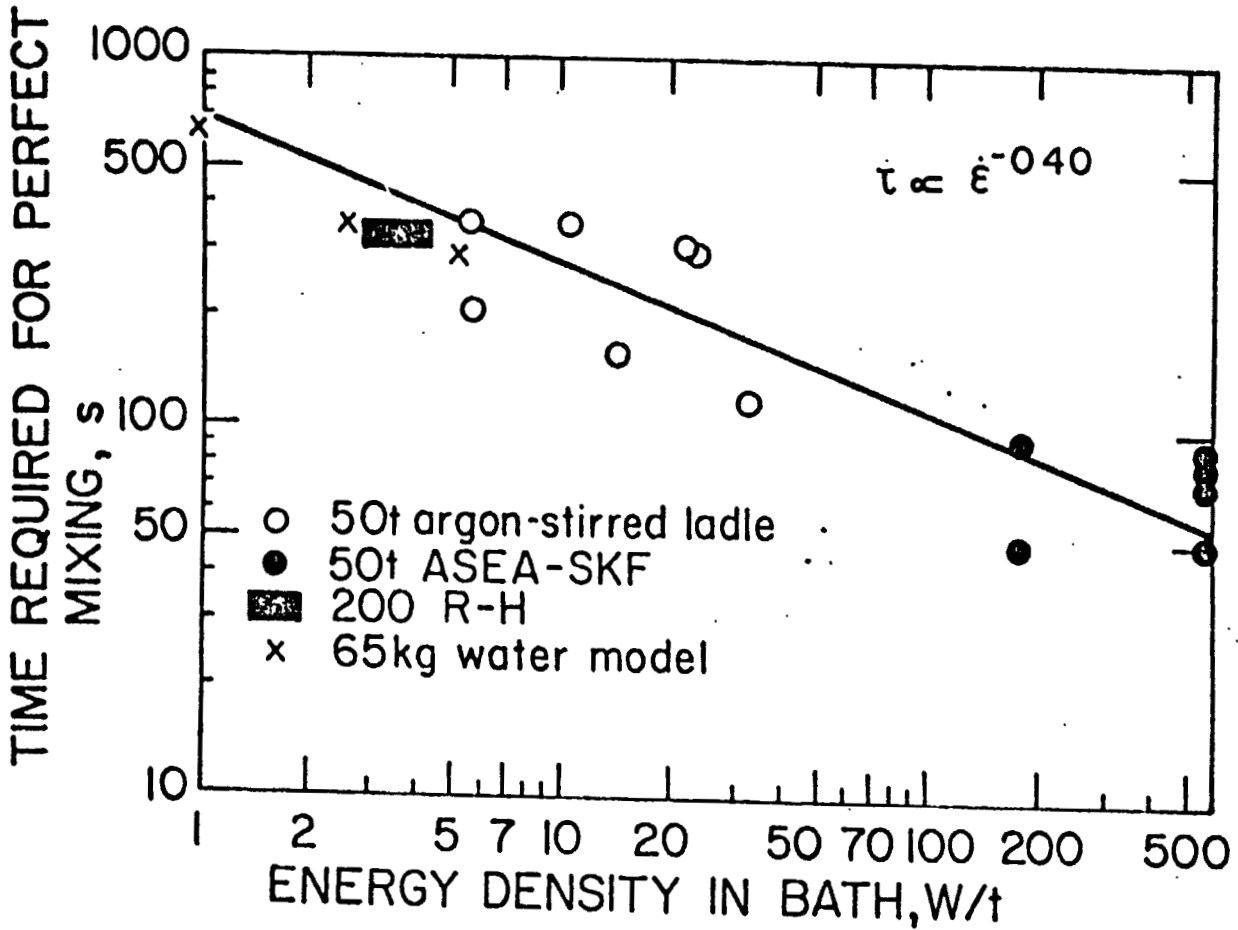
Fig. 1 Relationship between time required for complete
mixing and τ_b and rate of dissipation of energy
density i in various steel processing operations.
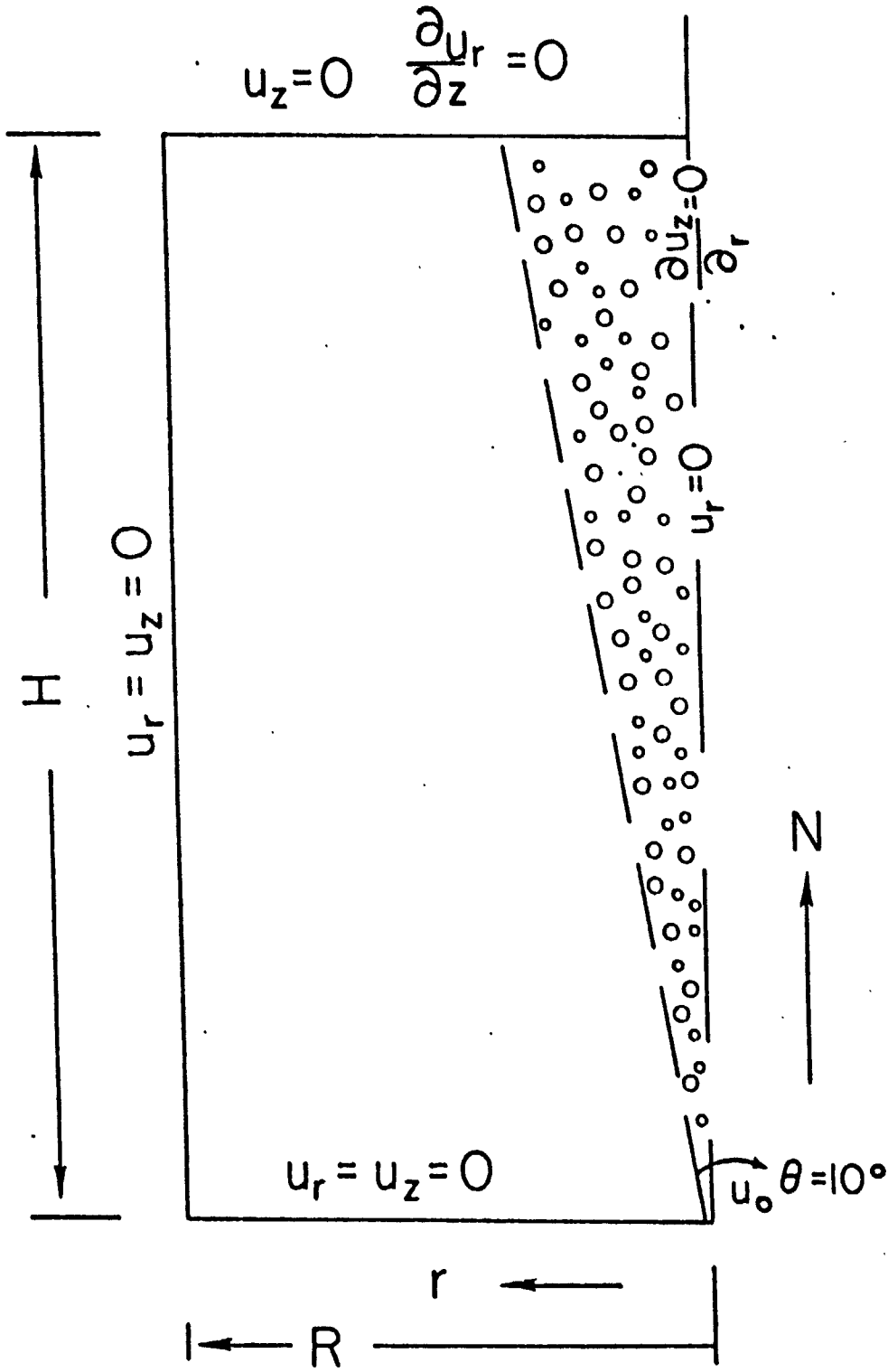
Fig. 2 Physical concept of the mathematical model.

Fig. 3 Schematic sketch of the apparatus

Photomultiplier
TSi Model 9160

Scattered Light
focusing lens —
TSi 935

Collecting lens-TSi 939
FL = 578 mm, ϕ_c = 4.909

Focusing lens-TSi 919
FL = 575 mm, ϕ_c = 4.919

Frequency shifter-TSi 980

Beamsplitter — TSi 915-2

Laser Source—
Spectra Physics He-Ne 124A
λ_o = 6328 Å
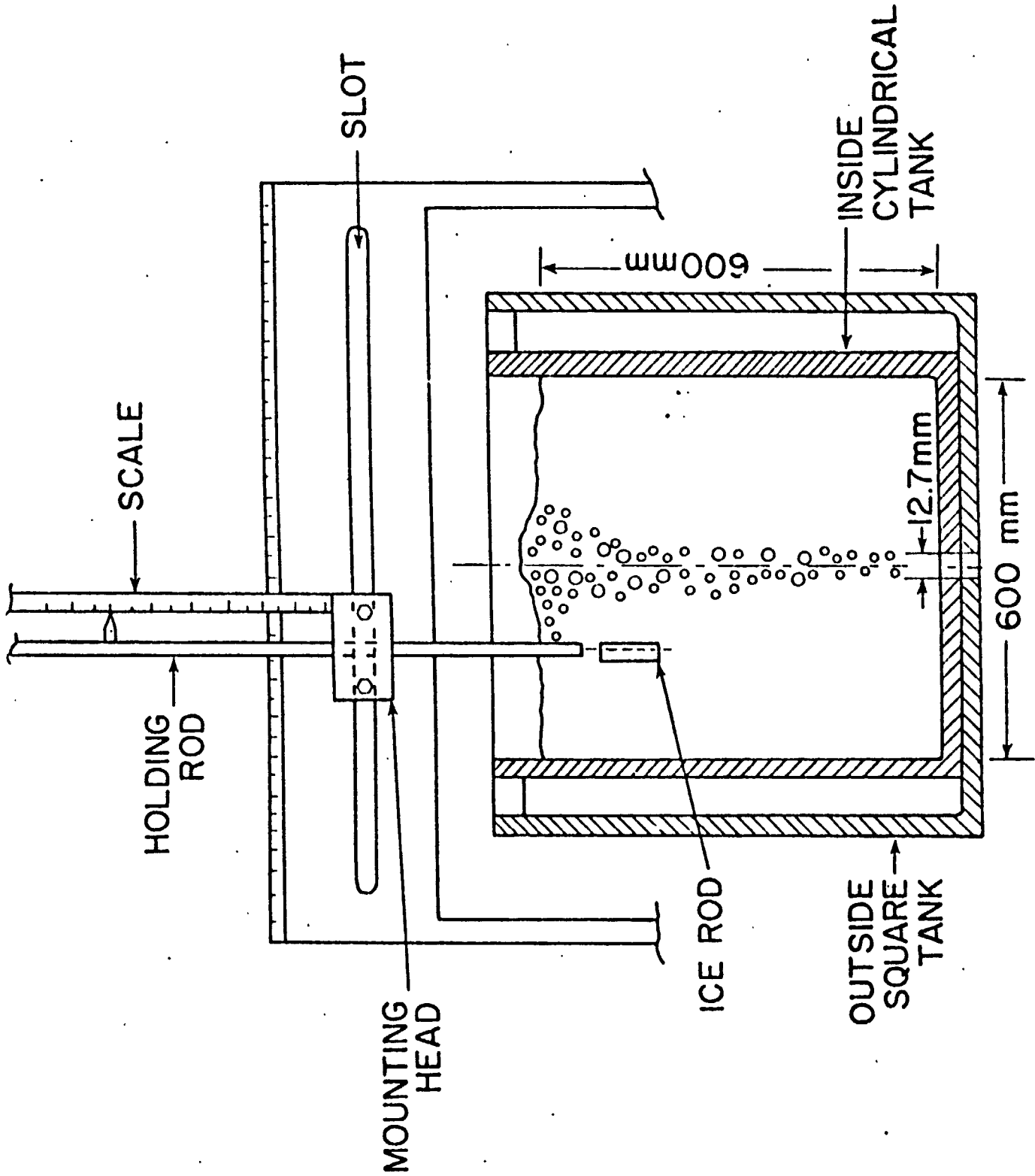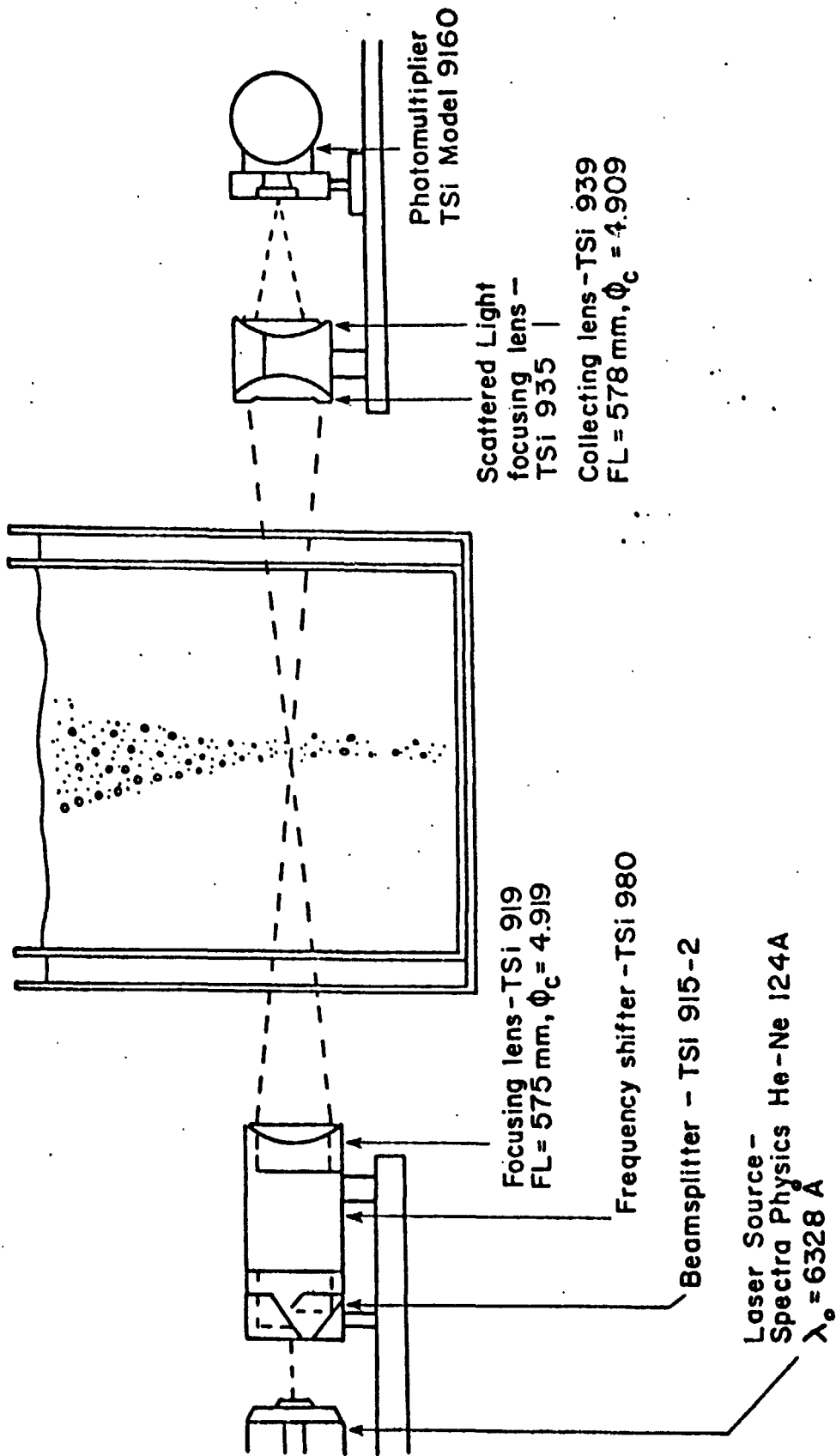
Fig. 4 LDA optical arrangement (Dual-Beam-Mode)
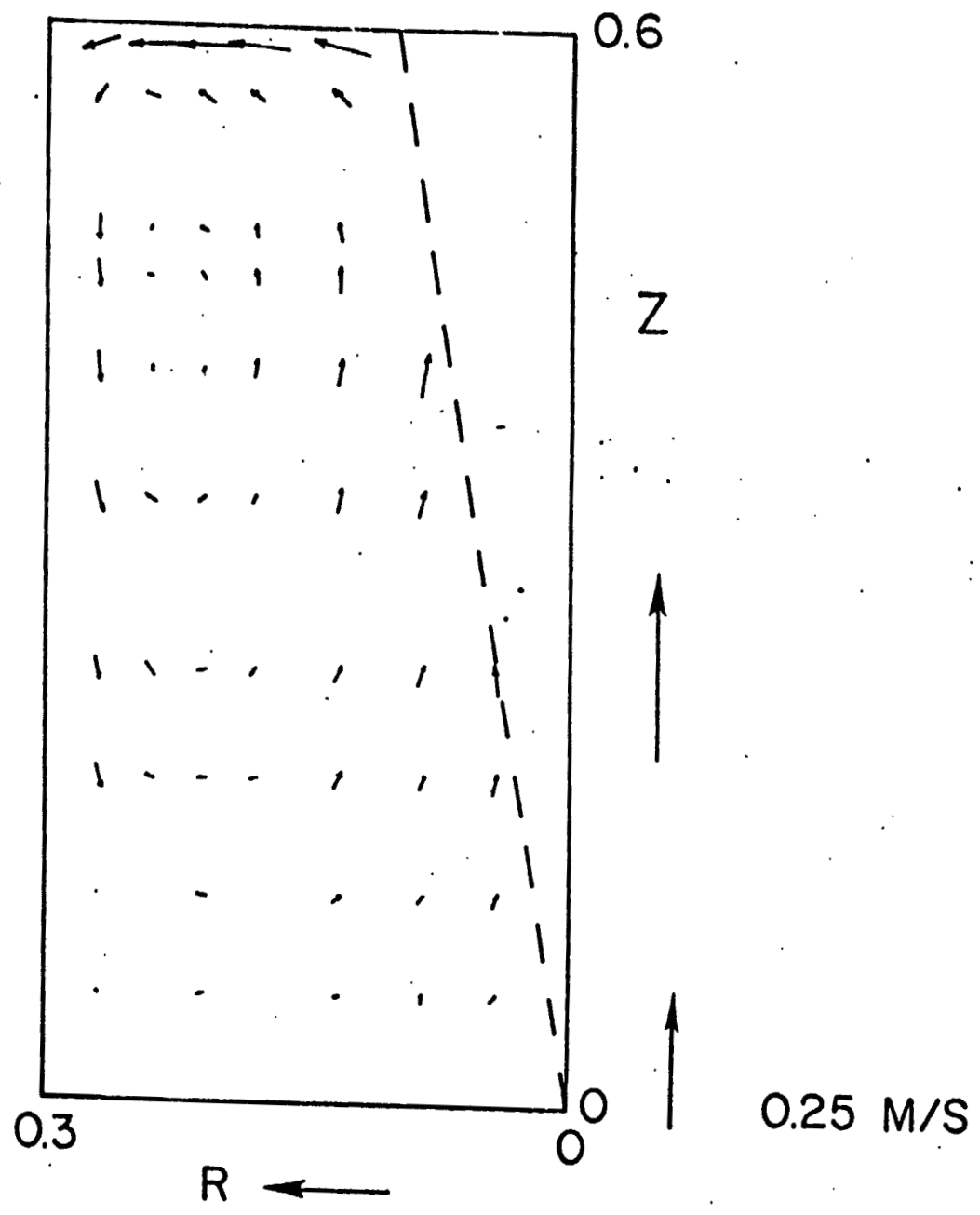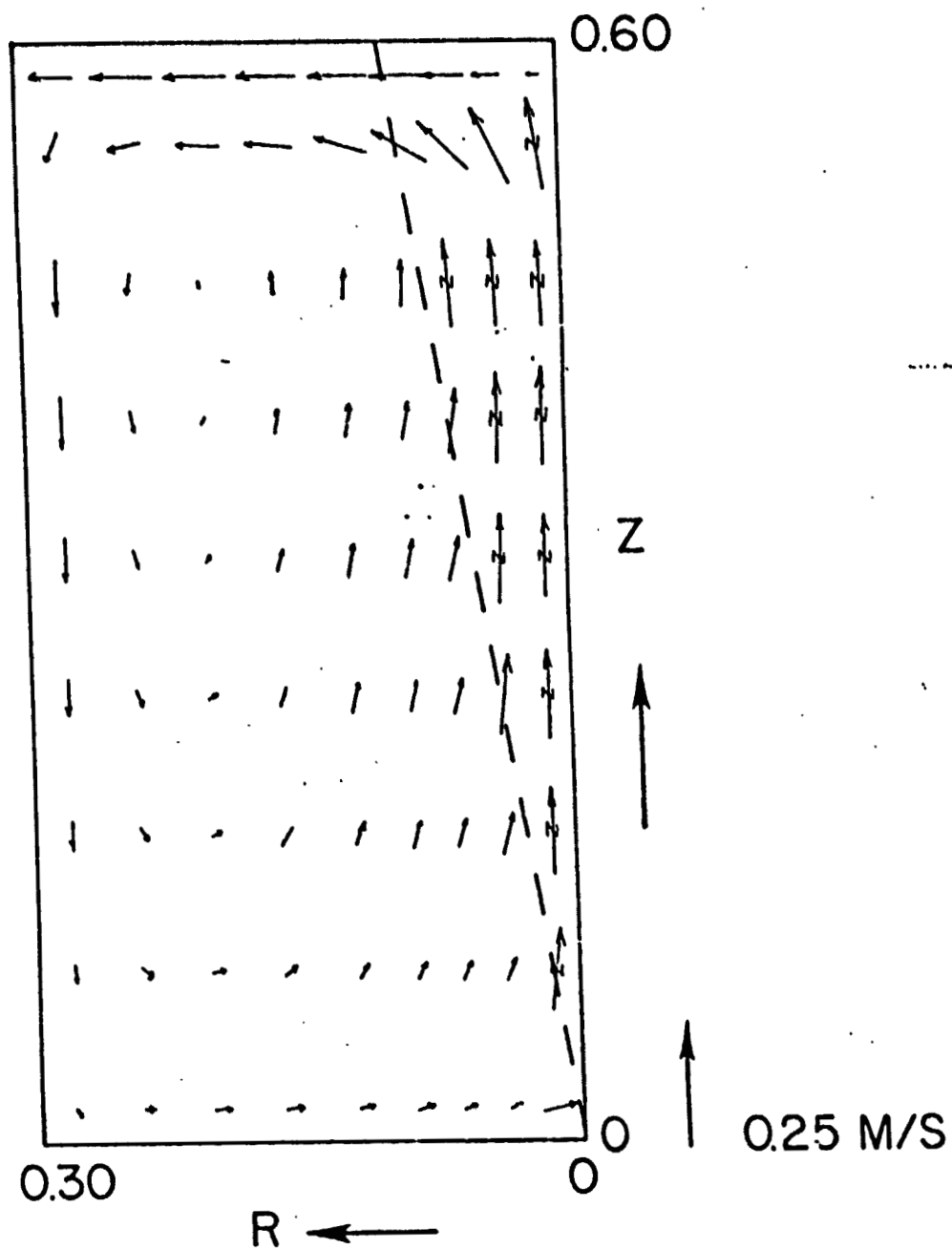
FIG. 5(a)

Fig. 5 A comparison of the experimentally measured and the computed velocity profiles for a linear gas velocity of 1.6 m/s at the orifice. (b) experimental measurements (b) theoretical predictions.
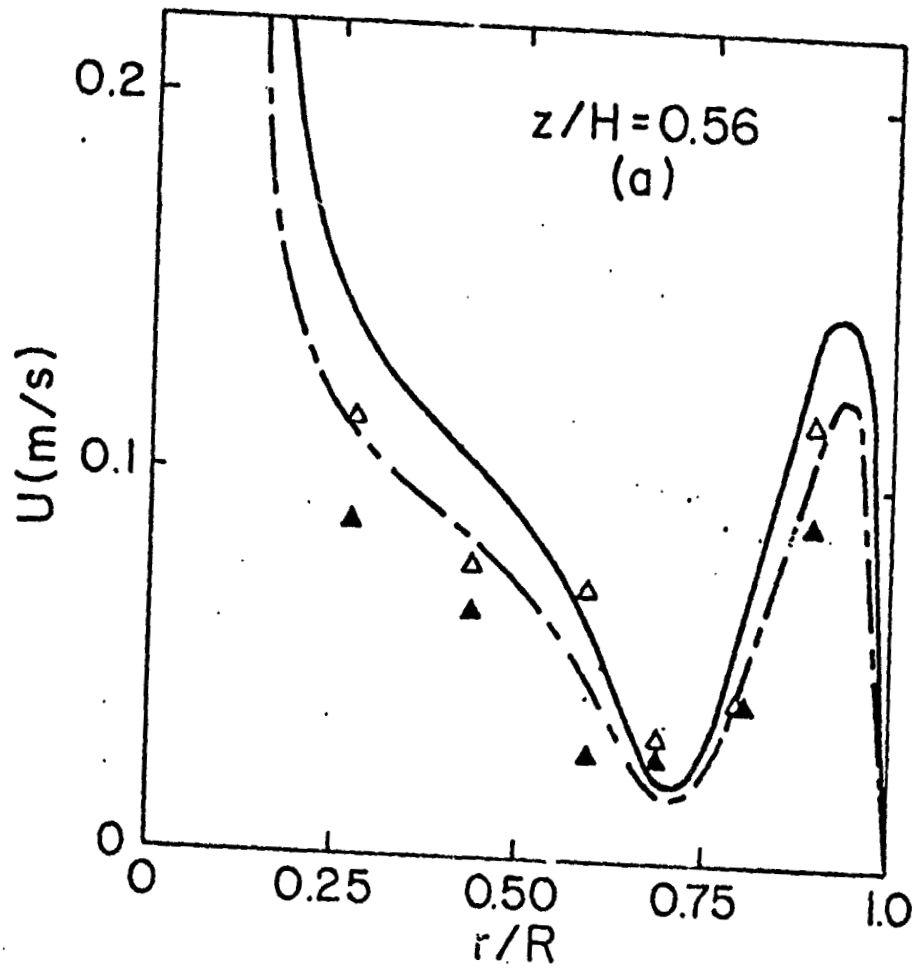
z/H = 0.56
(a)

Fig. 6a
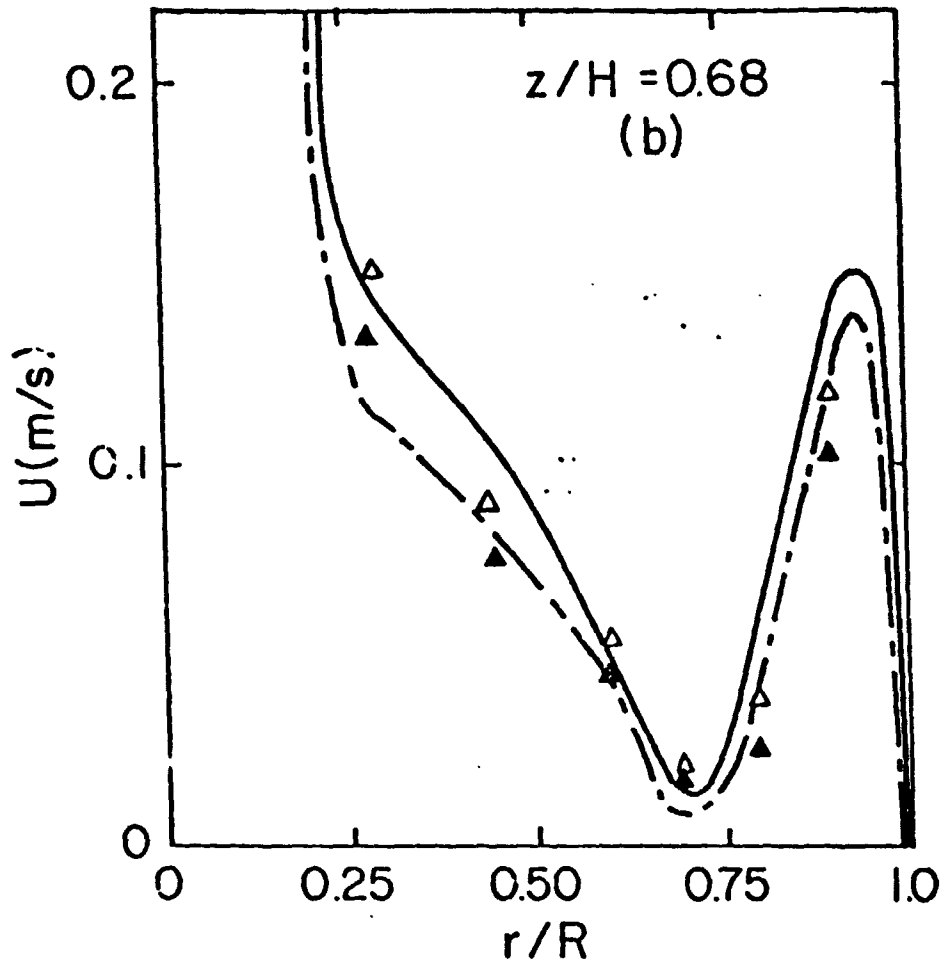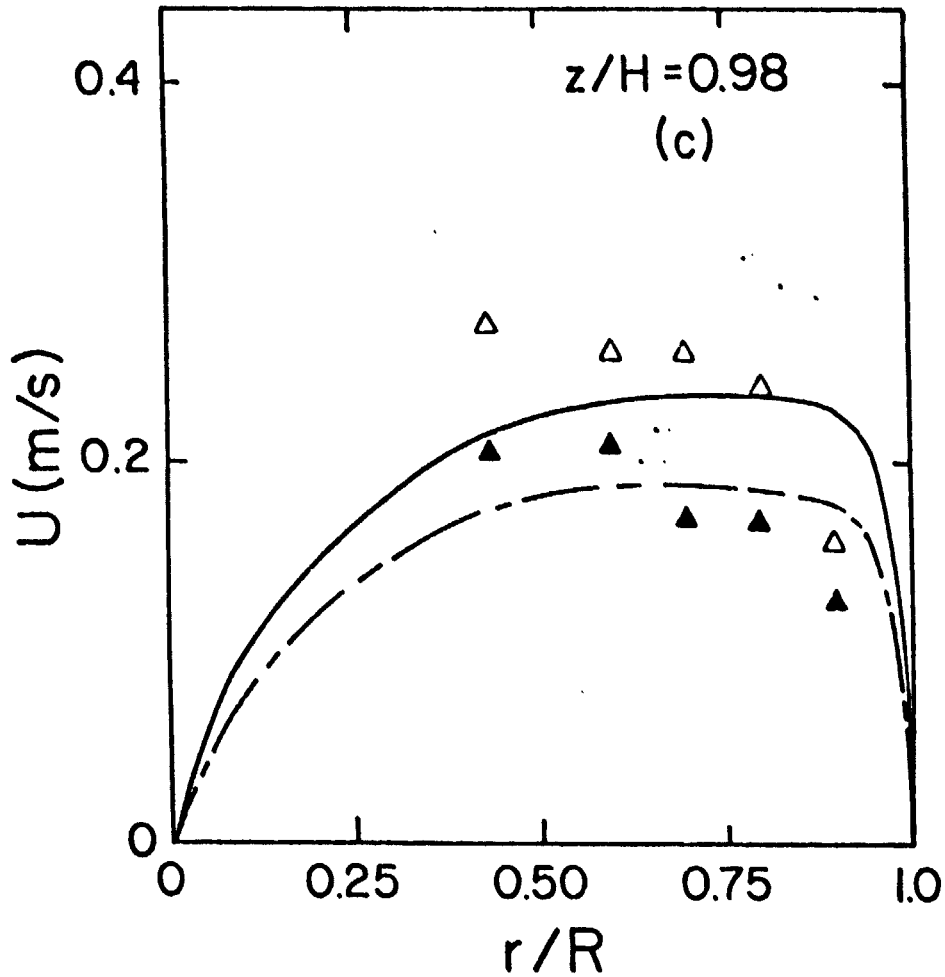
Fig. 6 The radial dependence of the absolute value of the velocity vector - a comparison of the predictions with measurements at various axial positions. Experimental measurements for an orifice velocity of 162 cm/s (▲) and 320 cm/s (△). Theoretical predictions for an orifice velocity of 162 cm/s (- . -) and 320 cm/s (———).
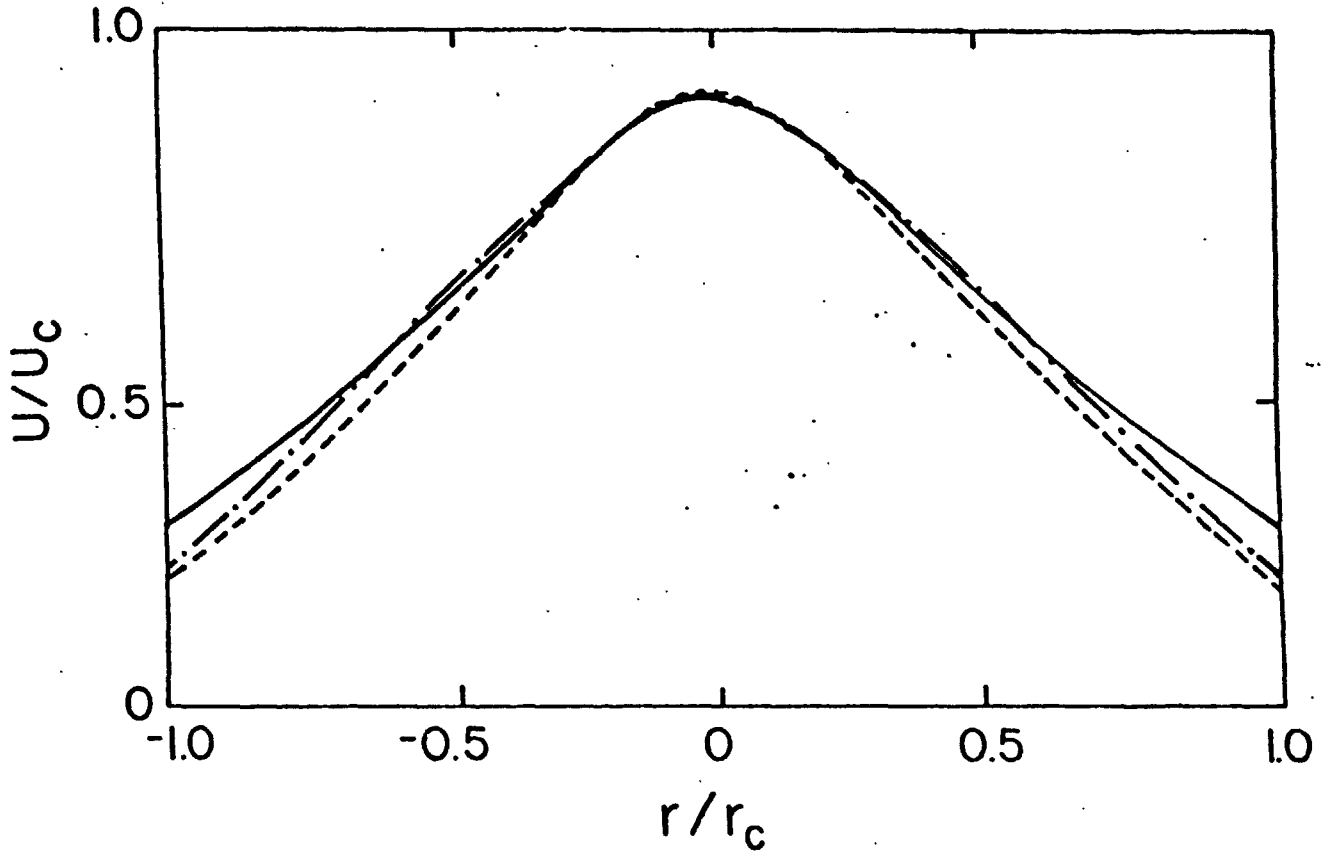
Fig. 7   The predicted radial variation of the normal velocity
in the jet cone region for various axial positions:
z/H=0.85 cm(———), z=0.60 cm(— — — —), and
z=0.33 cm (——— . ———).
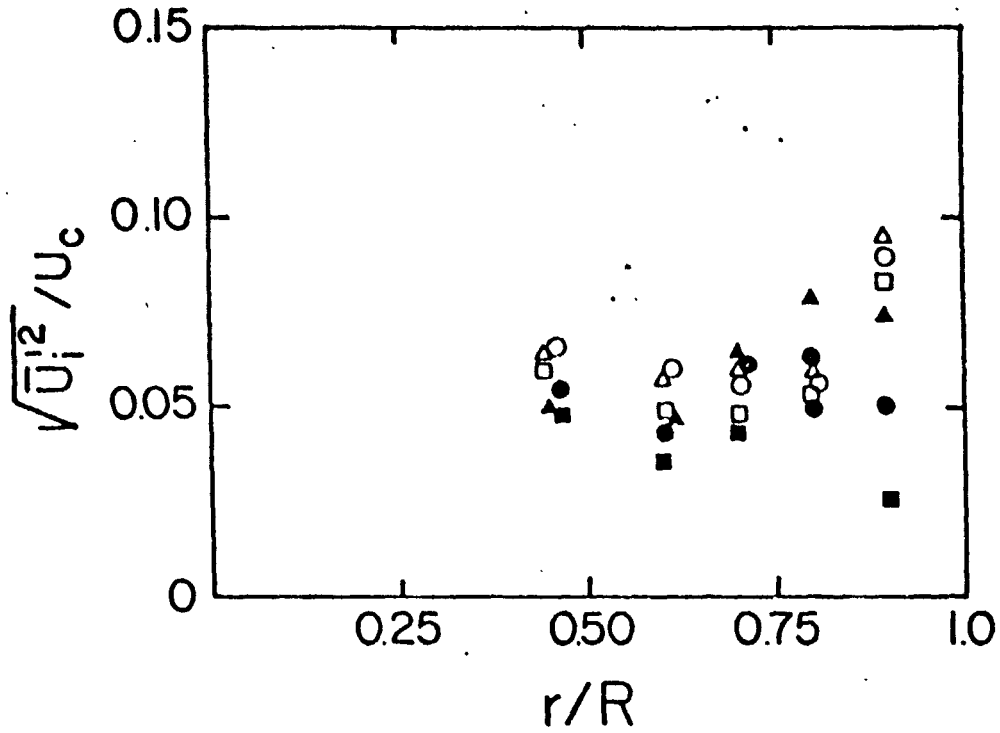
Fig. 8 The radial variation of the rms velocity components for an orifice velocity of:

$$1.62 \text{ m/s } \sqrt{\overline{U_z'^2}}/U_c, \sqrt{\overline{U_r'^2}}/U_c, \sqrt{\overline{U_o'^2}}/U_c \text{ for } z/H=.68(\triangle, \blacksquare, 0)$$

and $z/H=.40(\triangle, \blacksquare, 0)$
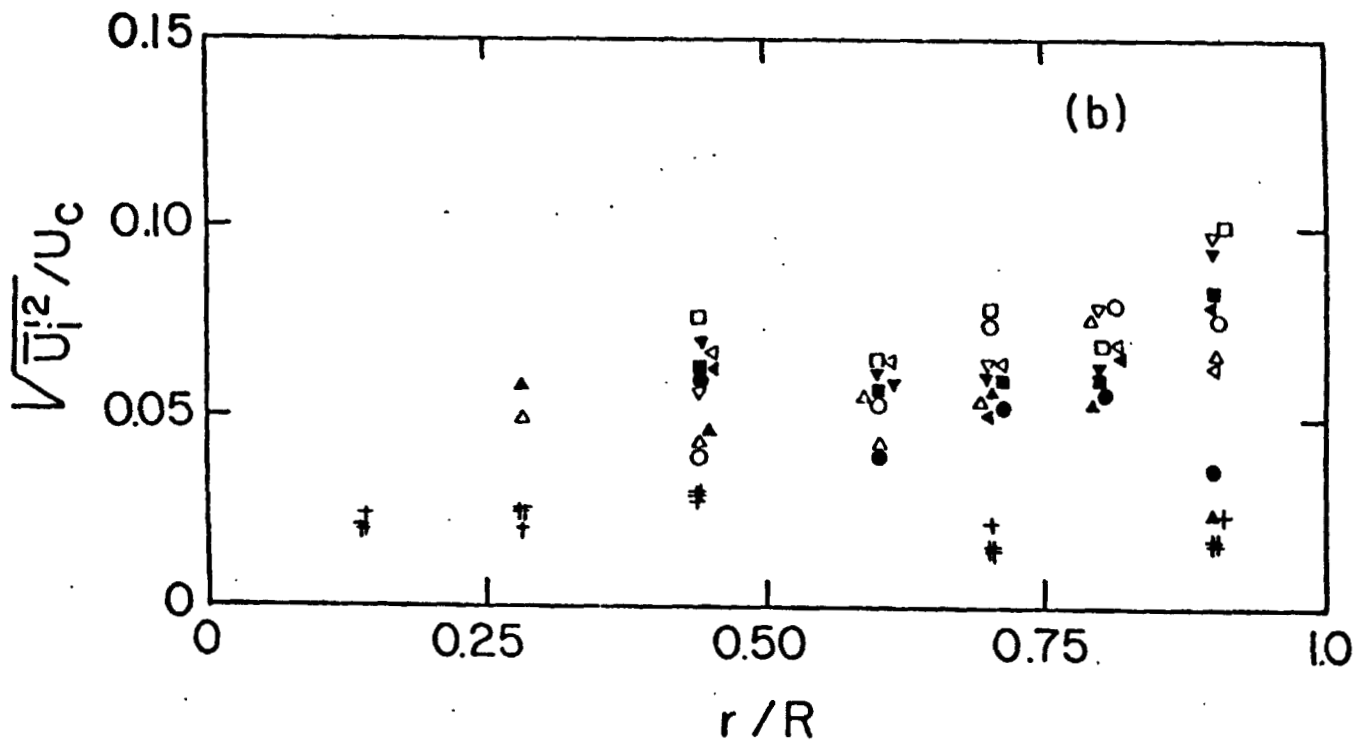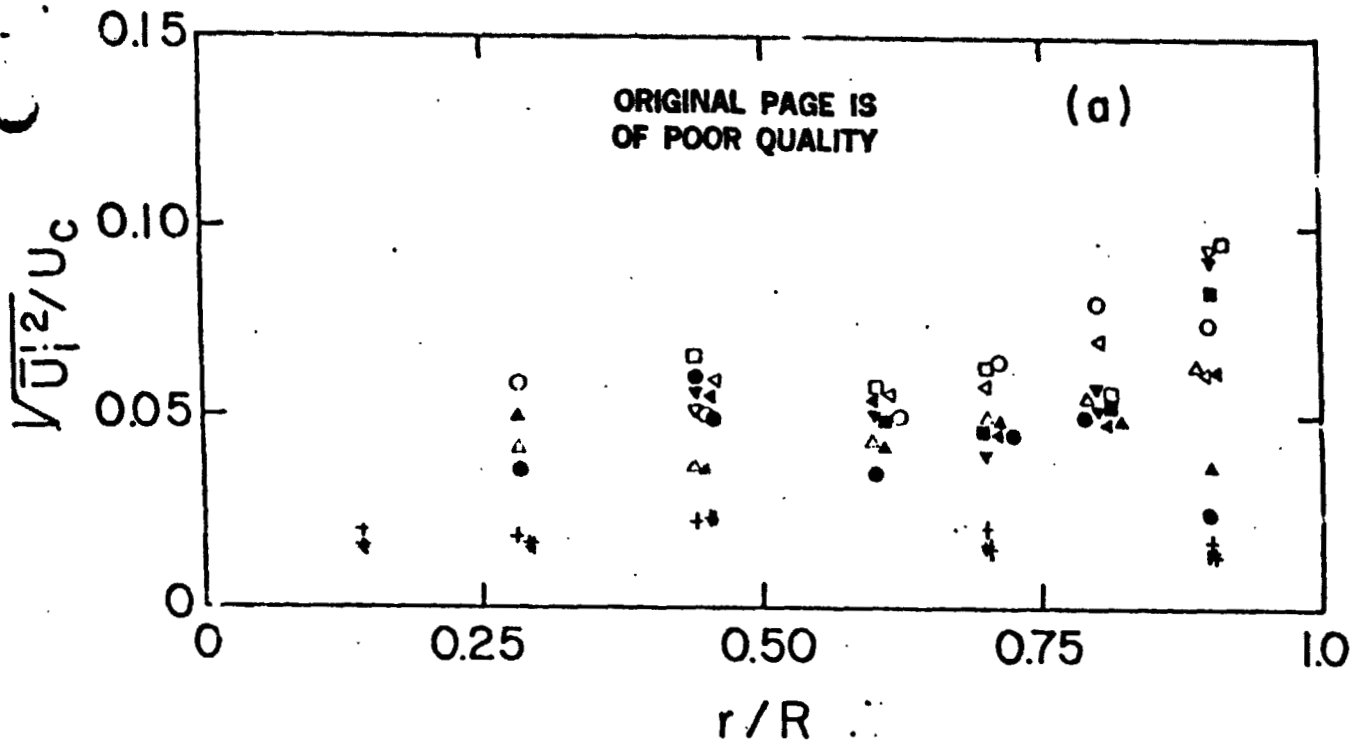
Fig. 9 The experimentally determined, normalized radial profile of the
rms velocity components. (a) linear orifice velocity 1.62 m/s;
(b) linear orifice velocity 3.20 m/s;

Notation: ⌐─── and ⌐─── for z/H=0.81(∇,▽)
$\sqrt{\overline{u_z'^2}}$ $\sqrt{\overline{u_r'^2}}$
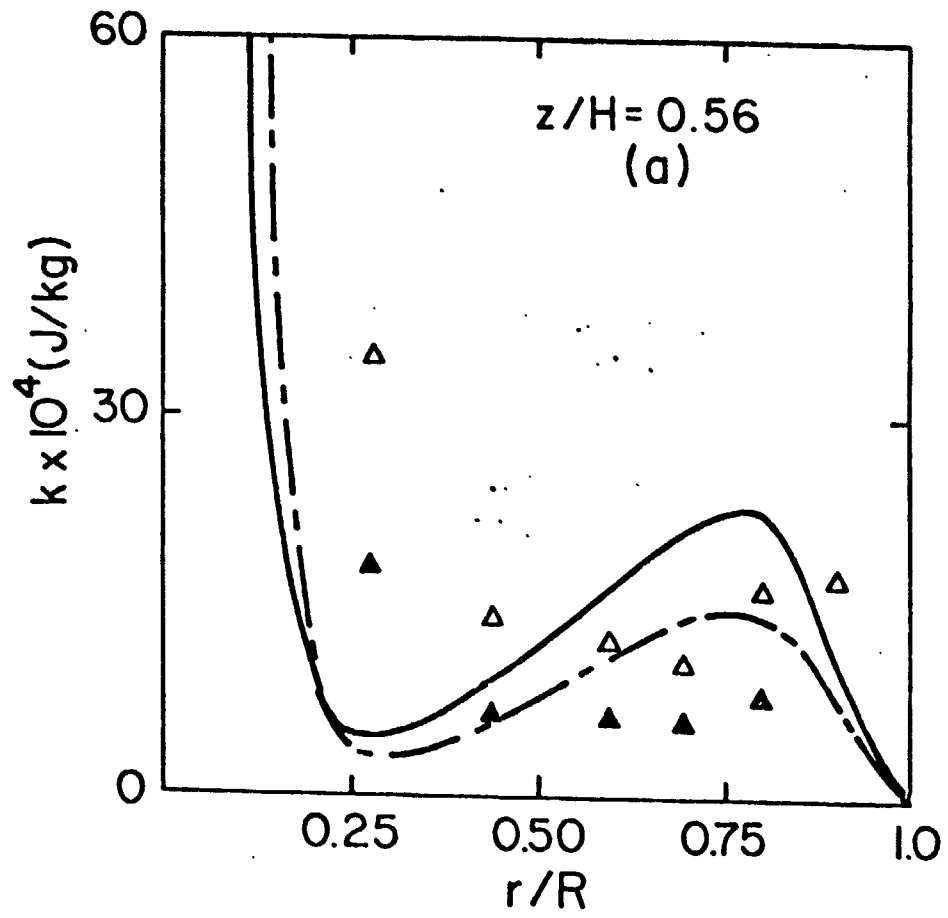
0.68(▬,▬), .56(∇ ▼),0.40(○,●),0.30(△ ▲),0.10(+,#)
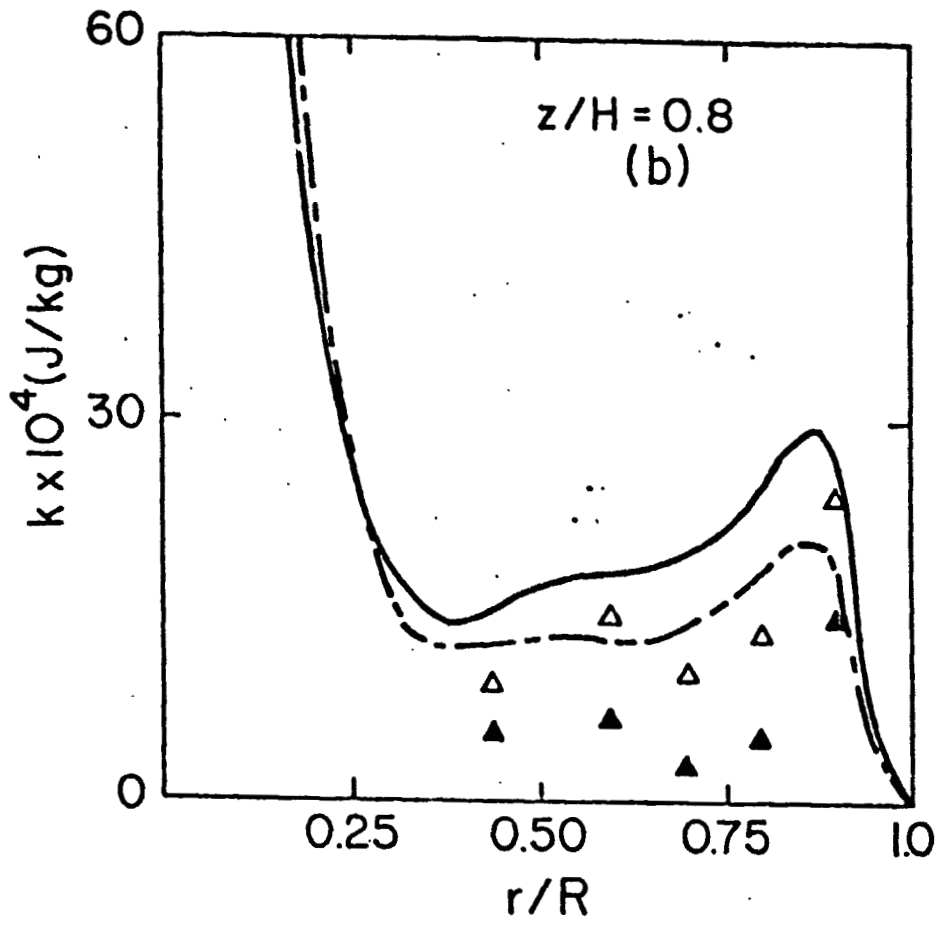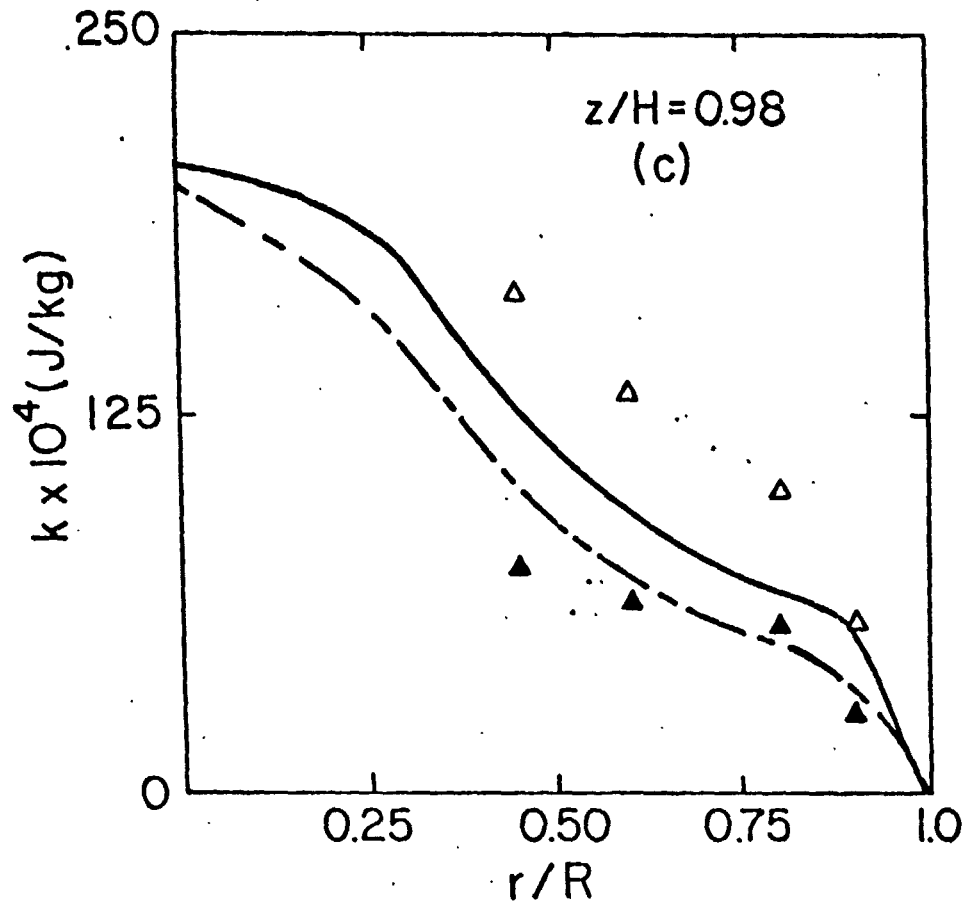
Fig. 10(a)

Fig. 10 (b)

Fig. 10 The radial variation of the turbulent kinetic energy - a
comparison of the measurements with predictions at various
axial positions. Experimental measurements for an orifice
velocity of 162 cm/s (▲ and 320 cm/s (Δ). Experimental
measurements for an orifice velocity of 162 cm/s (— — —)
and 320 cm/s (———)
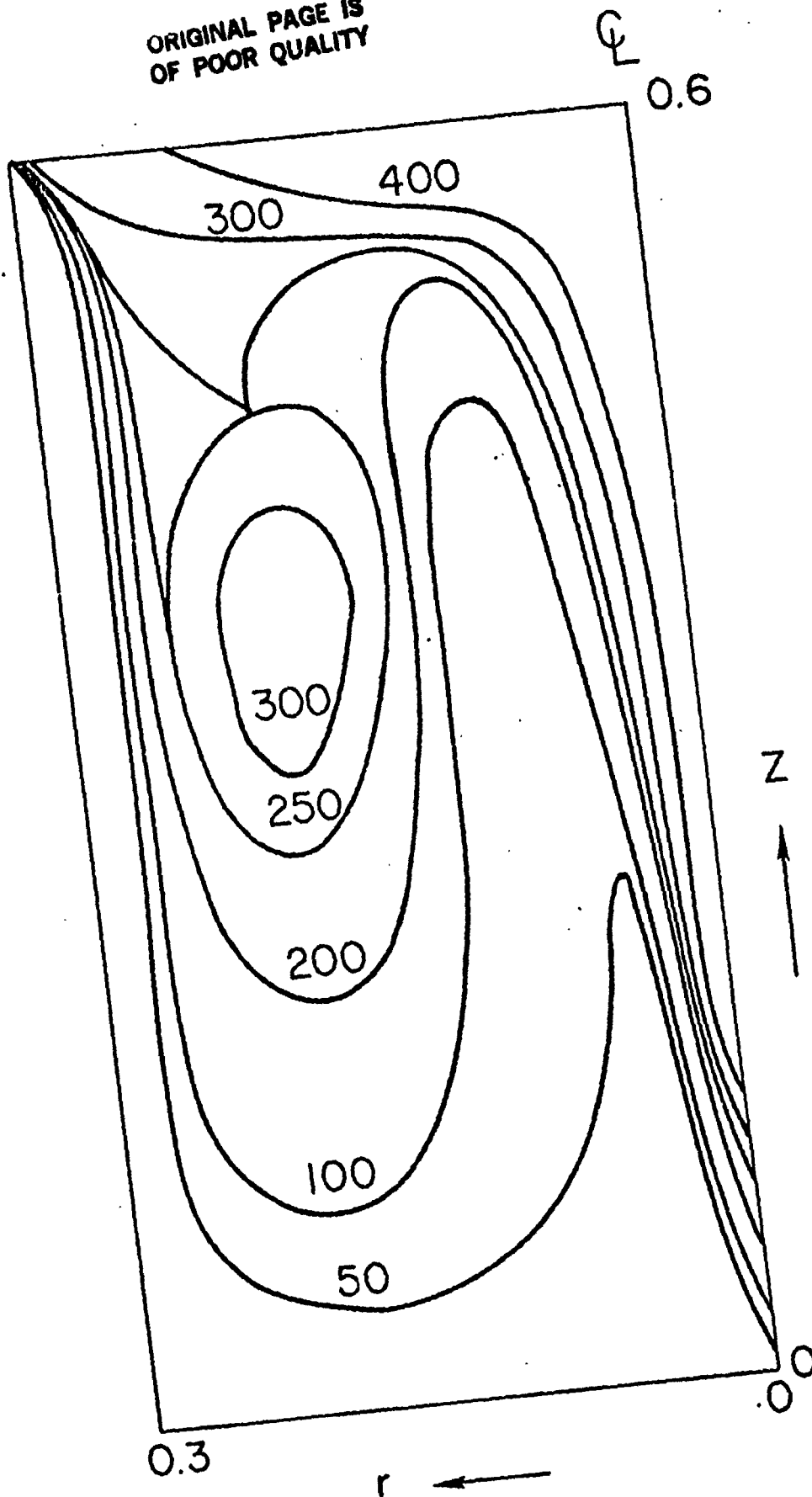
Fig. 11 The computed contours of the ratio: effective viscosity/
molecular viscosity. Air flow rate 1.6 m/s at the orifice.

t=40s
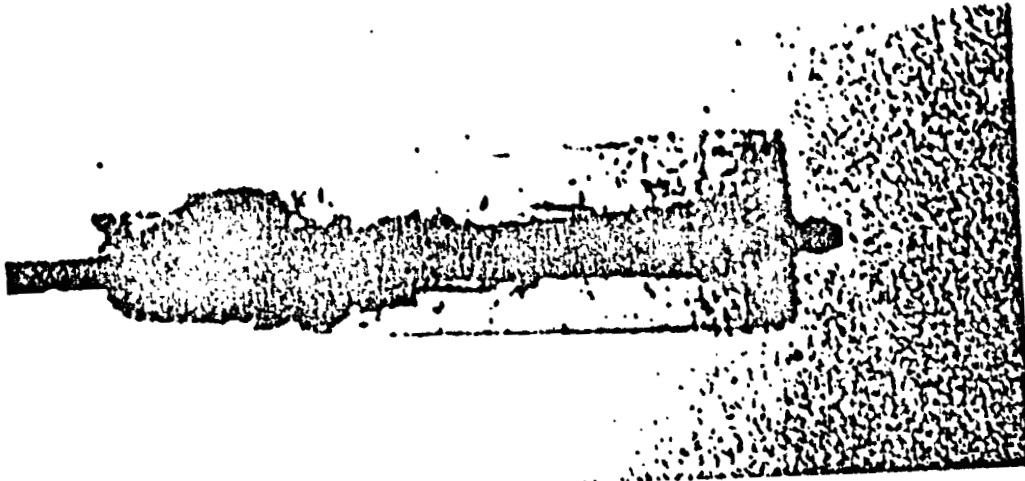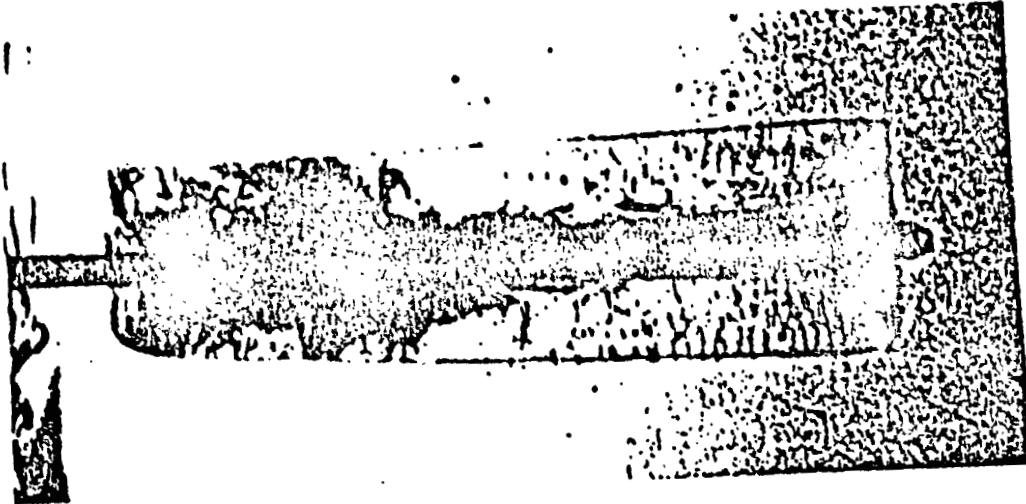
t=30s
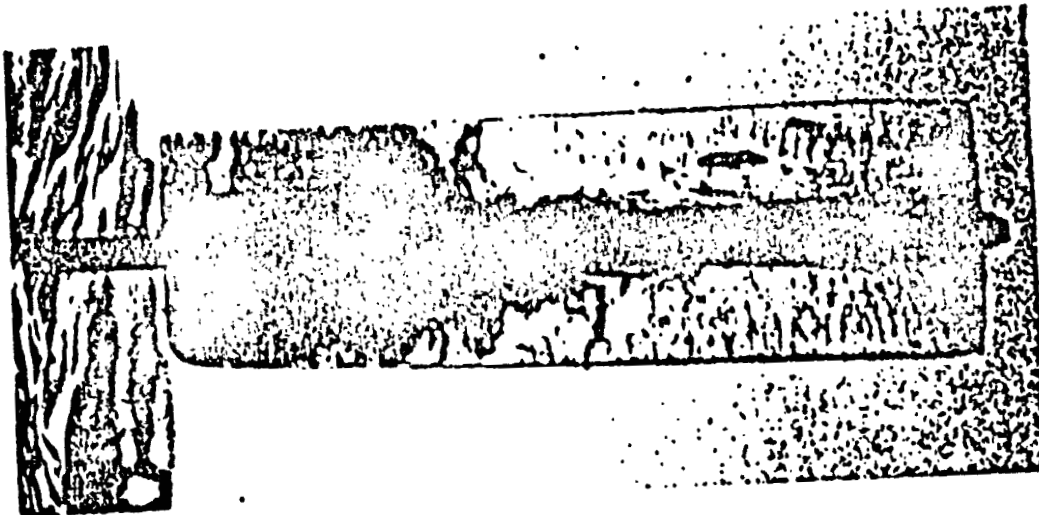
t=15s

Fig. 12 Melting sequence of the ice rod at position z/H=0.43.
r/R=0.90, U_o=1.62 m/s.
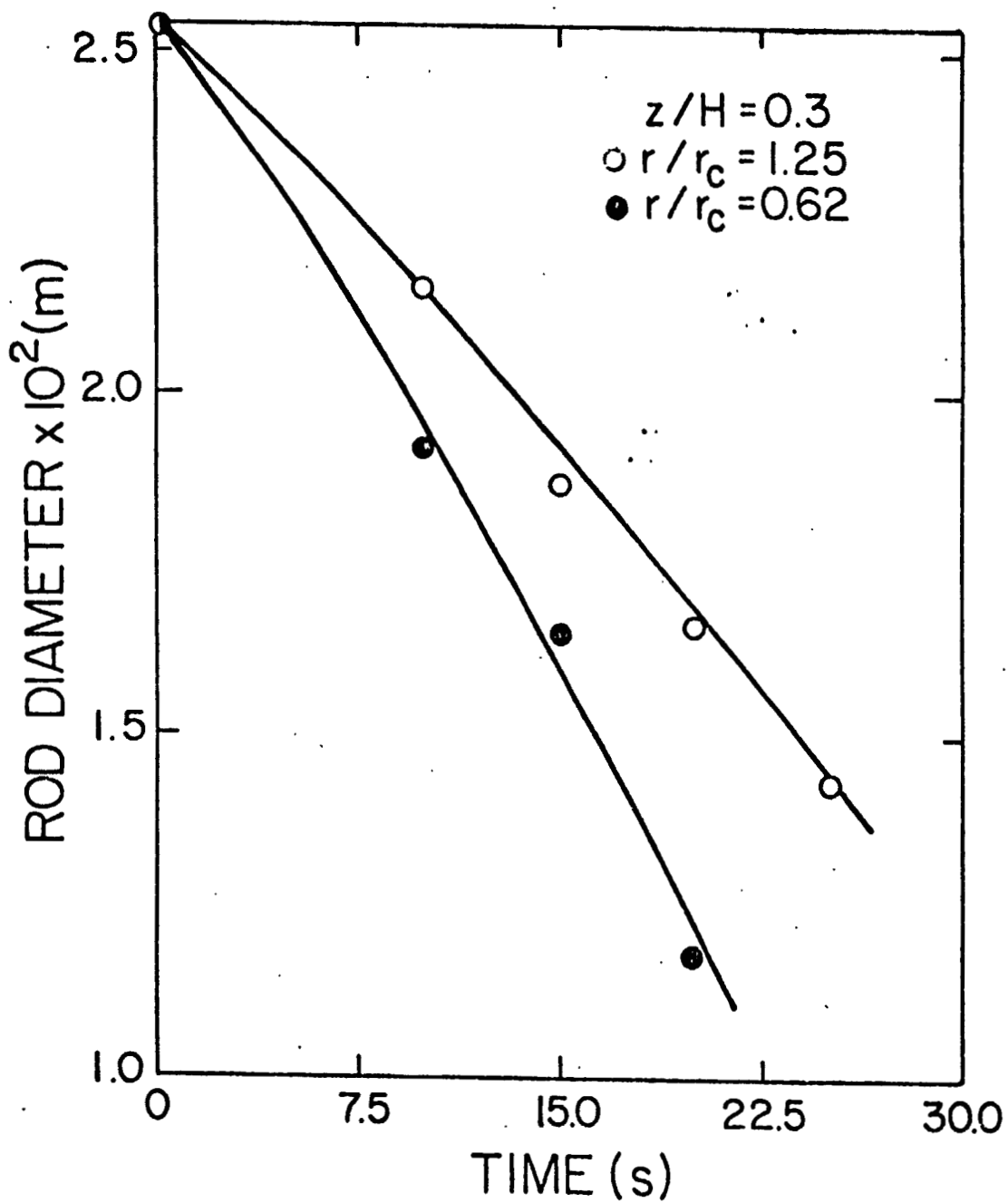
Fig. 13 Ice rod diameter vs. time at z/H=0.3

z/H=0.56

Melting Rate $\times 10^4$ (m/s)

Two phase region

r/R
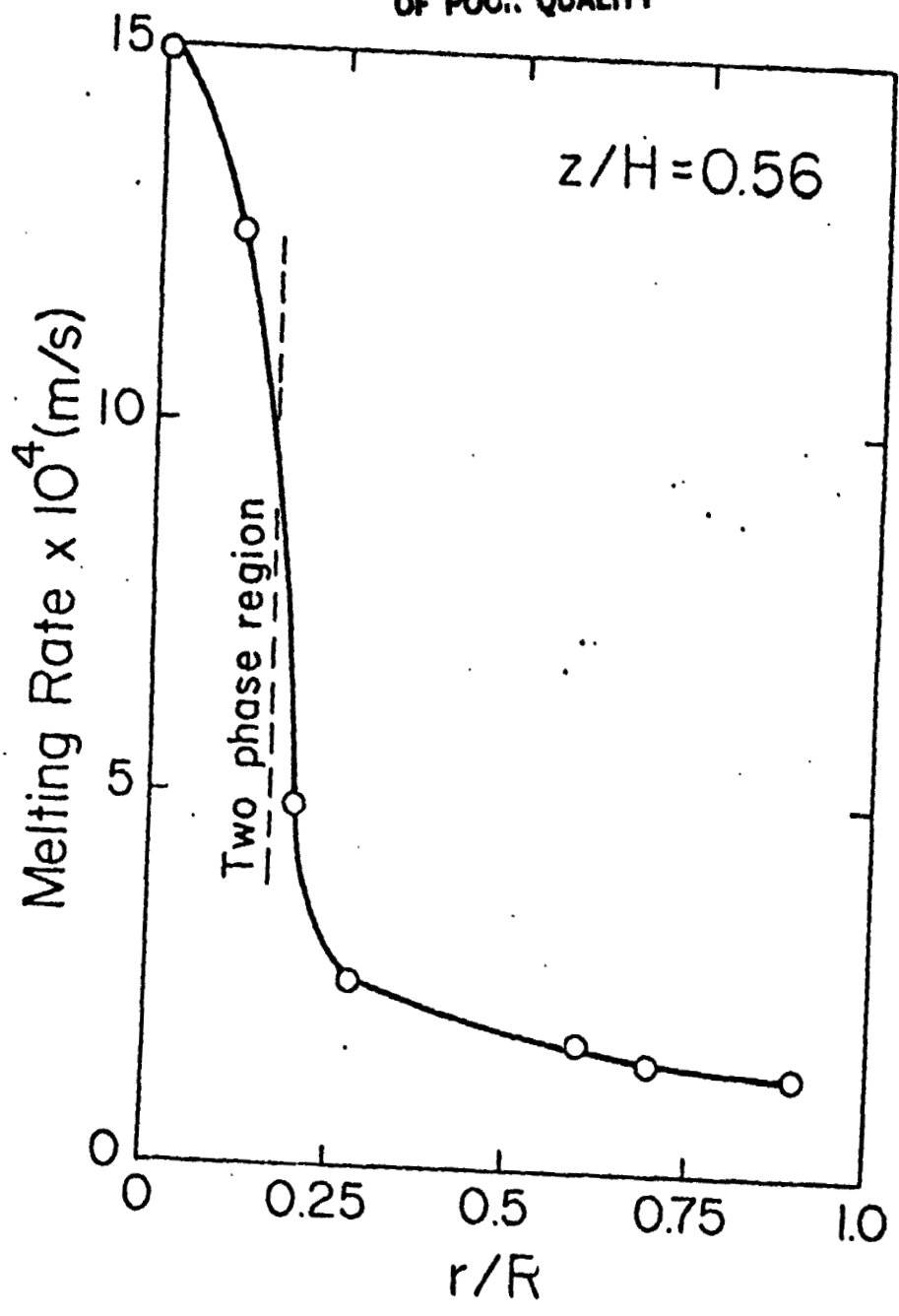
Fig. 14 Radial distribution of the initial rate at z/H=0.93
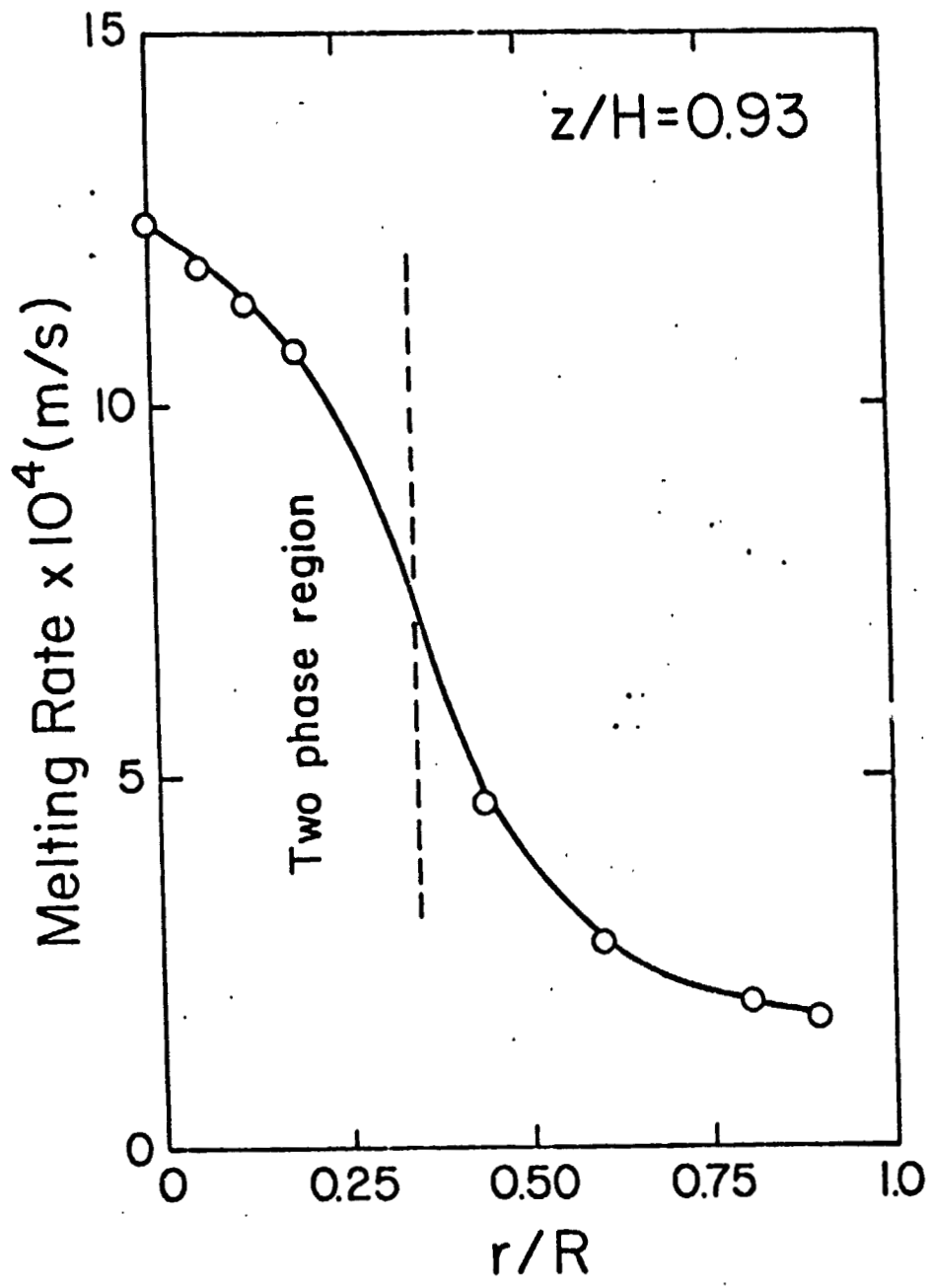
Fig. 15 Radial distribution of the initial melting
rate at z/H=0.56.
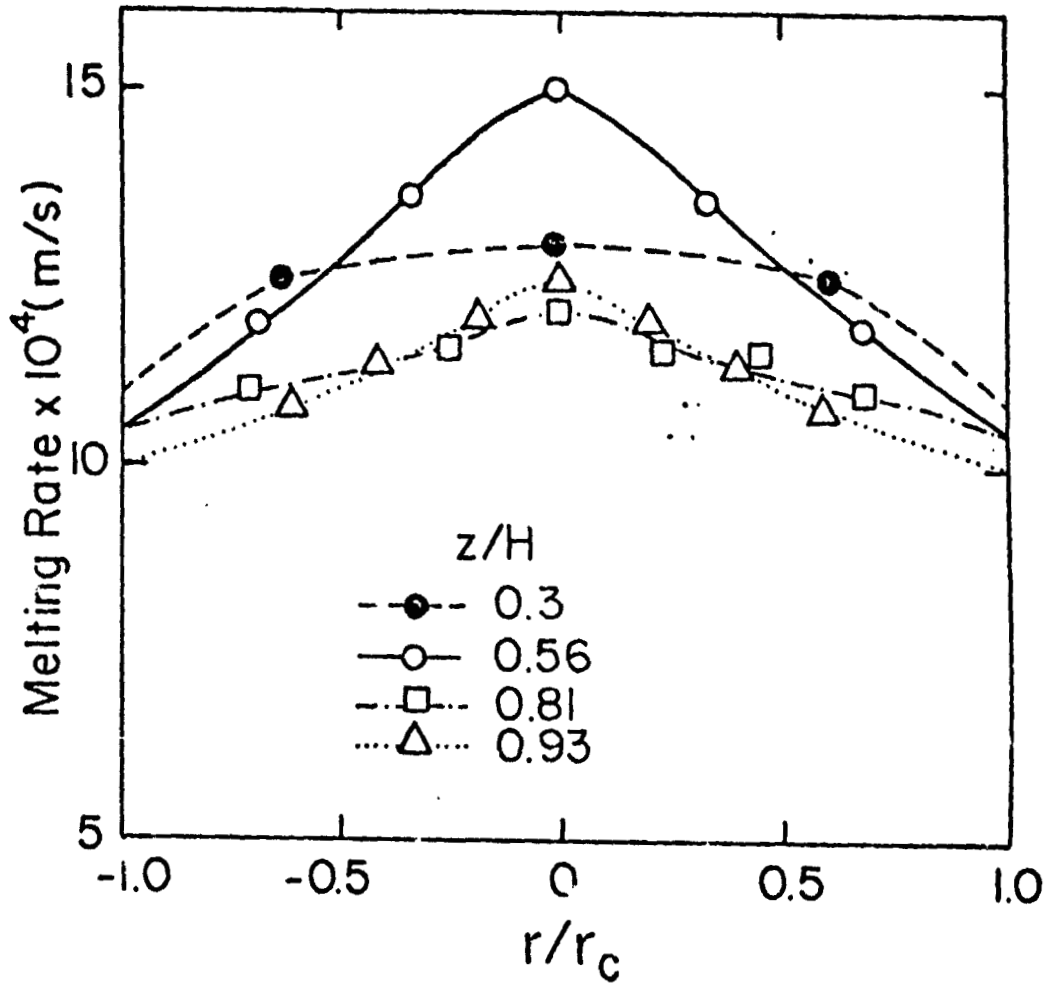
Fig. 16   Radial distribution of the initial melting rate in the
jet cone at different axial positions.
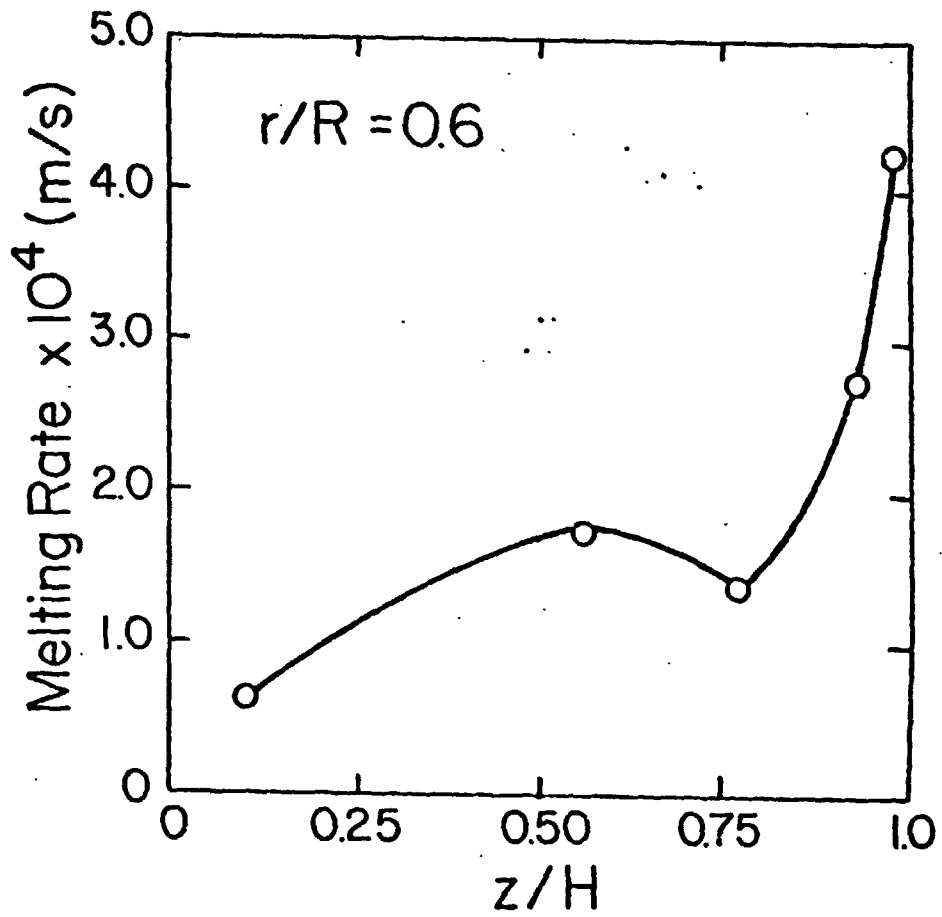
Fig. 17 Vertical distribution of the initial melting rate
at r/R=0.9.
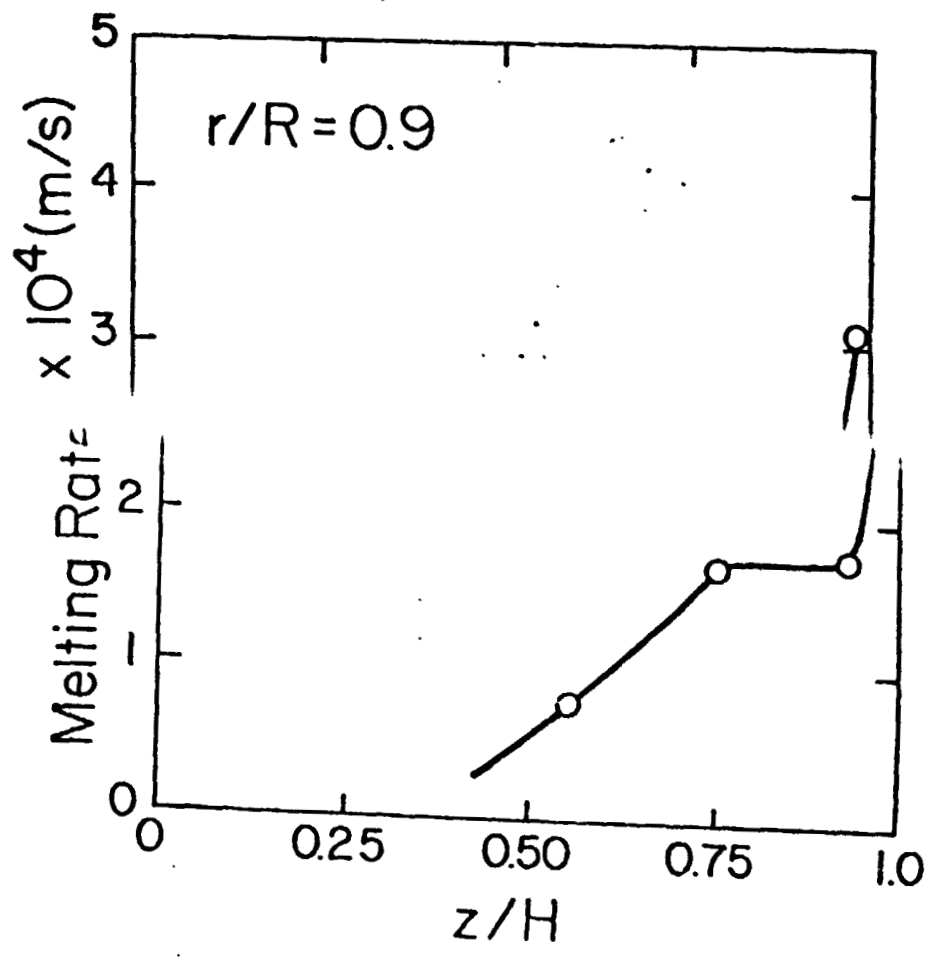
Fig. 18 Vertical distribution of the initial melting rate at r/R=0.6.
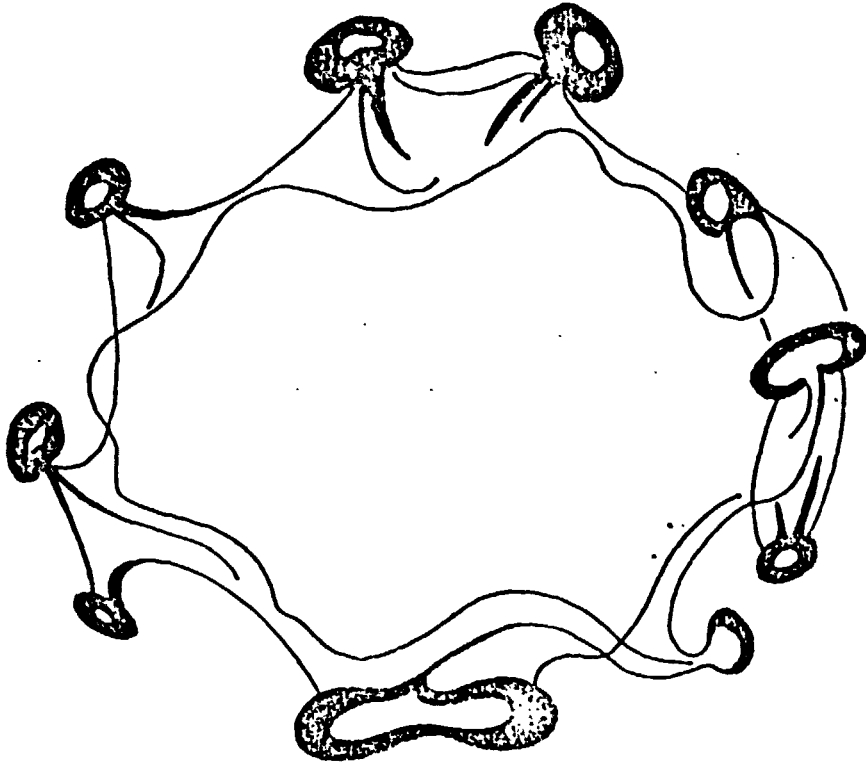
Fig. 19 Schematic sketch of the tracer dissipation as
affected by the eddies.
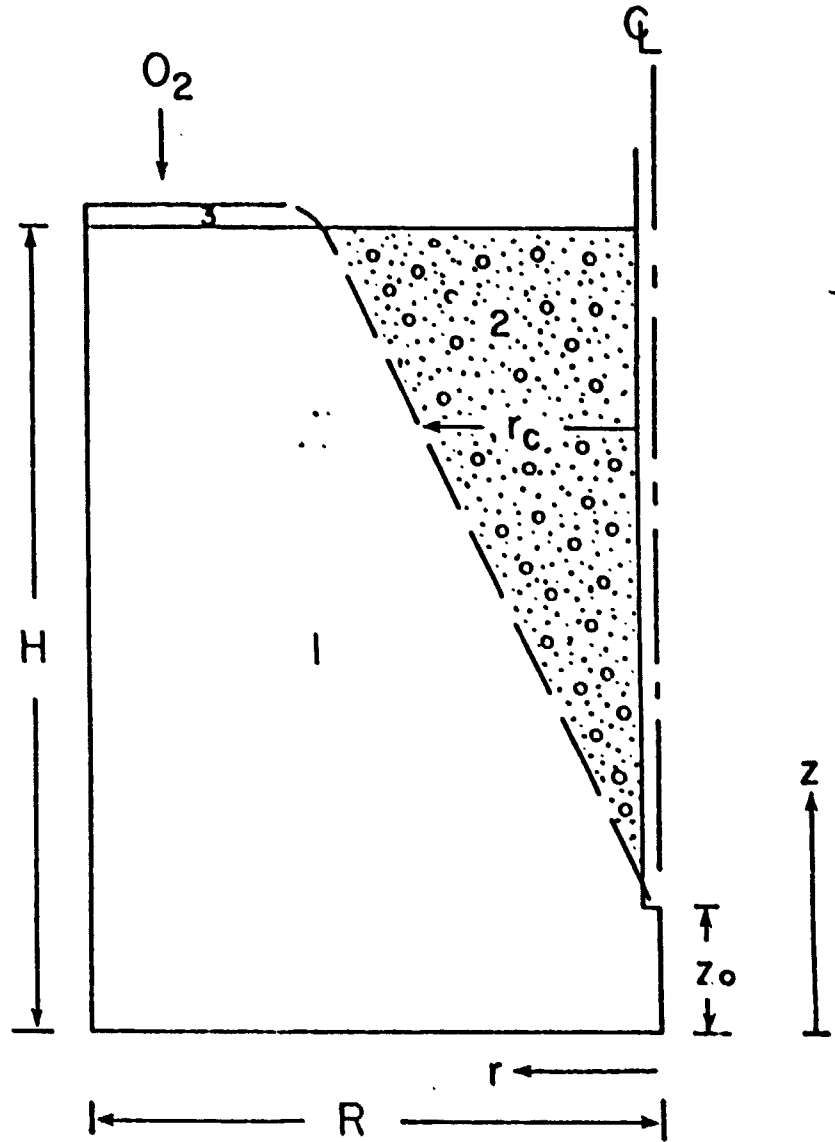
Fig. 20 Schematic representation of the desulfurization model,
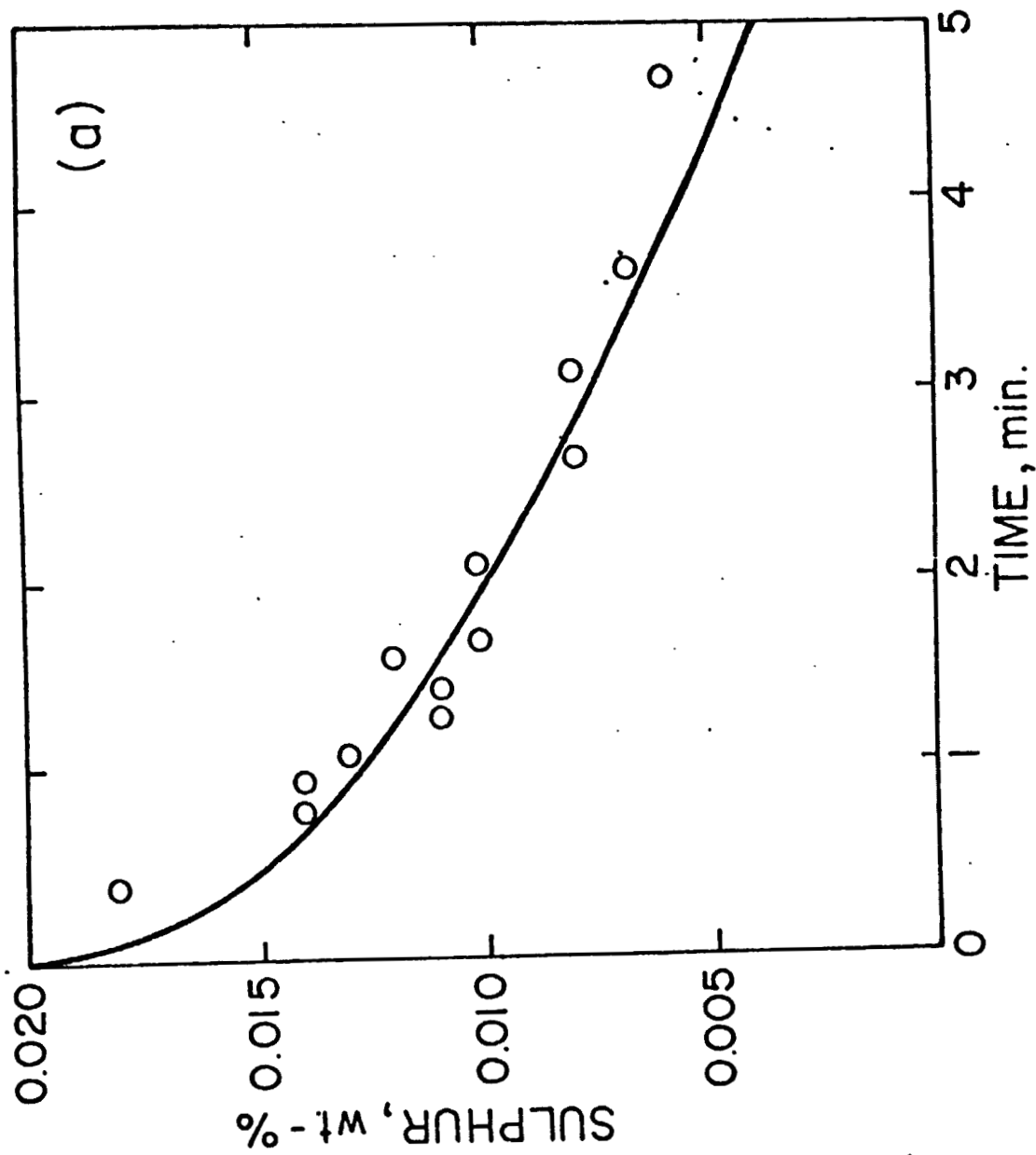1-molten steel, 2-the three phase zone, 3-slag layer.
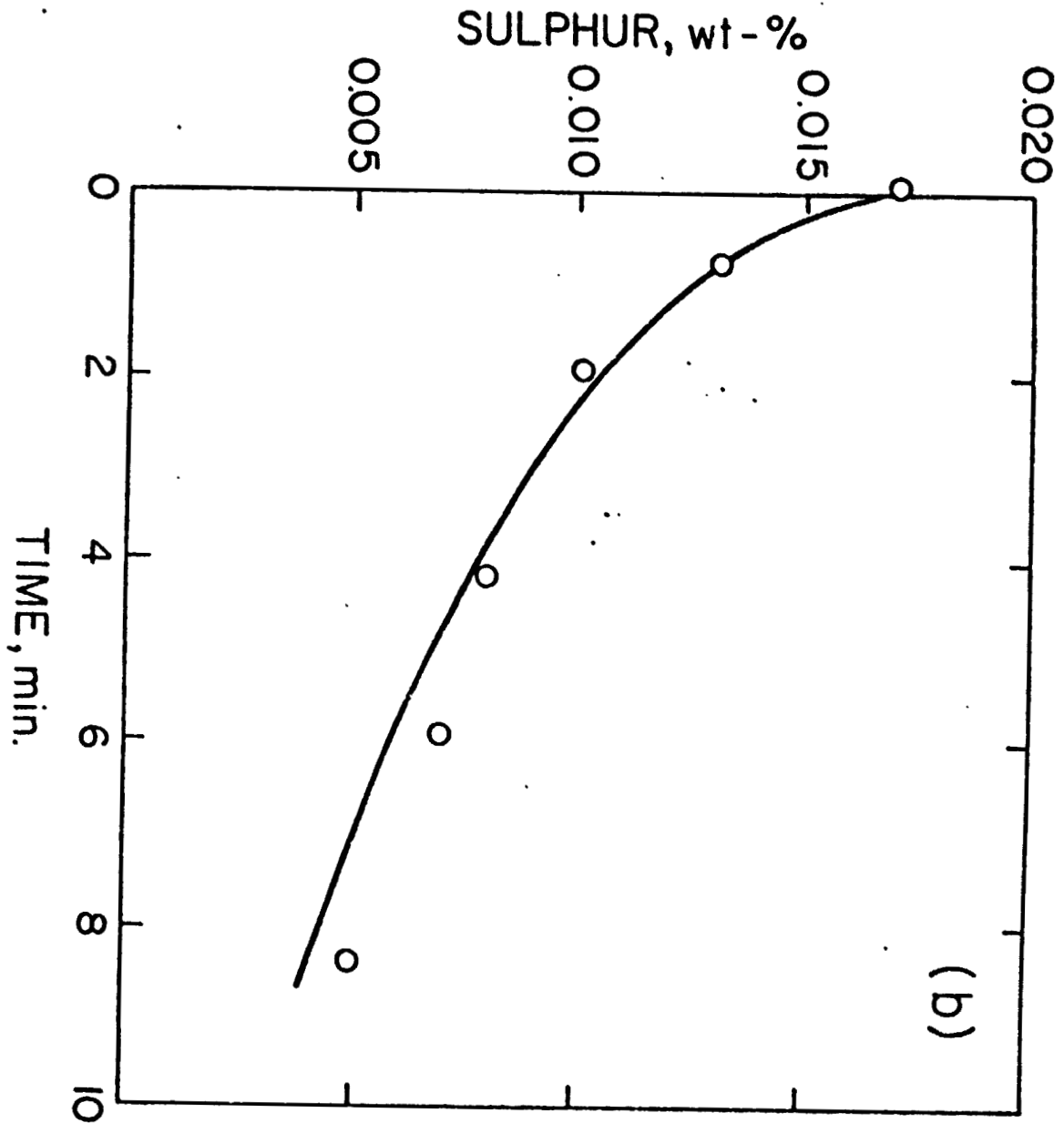
(a)

SULPHUR, wt-%

TIME, min.

Fig. 21 (a)

Fig. 21 Comparison between experimentally measured and theoretically predicted sulfur content in Argon-Stirred ladle as function of time. (a) 6 ton ladle; (b) 40 ton ladle.

Fig. 22 Carbon electrodes in Argon-Stirred Ladle for measurements
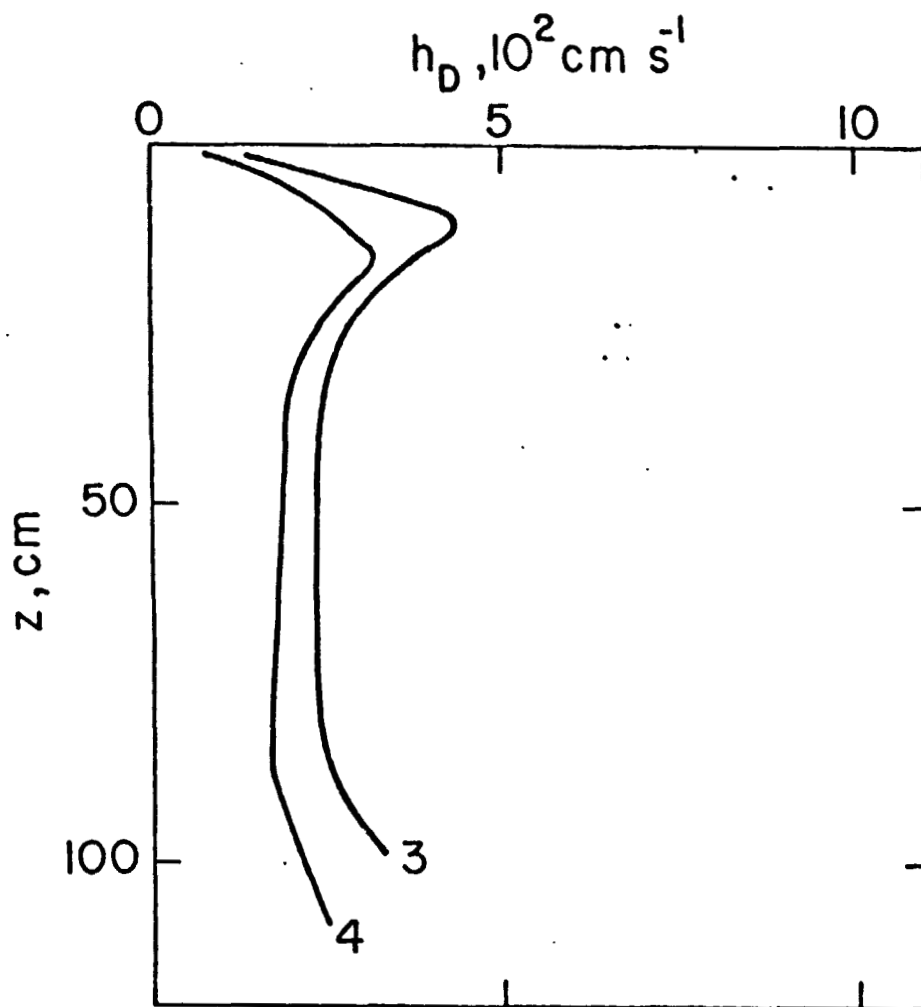of mass transfer rate.

Fig. 23 Measured values of mass-transfer coefficient
for carbon dissolution showing effect of immersion
depth and location.